Radio Frequency Photonic In-Phase and Quadrature-Phase Vector Modulation

A Thesis
Presented to
The Academic Faculty

By

Kyle Davis

In Partial Fulfillment
Of the Requirements for the Degree
Master of Science in Electrical Engineering

Georgia Institute of Technology
December, 2013

Radio Frequency Photonic In-Phase and
Quadrature-Phase Vector Modulation

Approved by:

Dr. Stephen E. Ralph, Advisor
School of Electrical and Computer Engineering
Georgia Institute of Technology

Dr. William D. Hunt
School of Electrical and Computer Engineering
Georgia Institute of Technology

Dr. Benjamin D. B. Klein
School of Electrical and Computer Engineering
Georgia Institute of Technology

Date Approved: November 12, 2013

ACKNOWLEDGEMENTS

The author would like to thank the committee members for many fruitful discussions and for their guidance throughout the preparation of this thesis. The author would also like to thank the Institute for the facilities and personnel that helped produce the results of this document.

TABLE OF CONTENTS

LIST OF FIGURES

List of Figures

SUMMARY

The focus of this thesis is to investigate the implementation of Radio Frequency (RF) In-Phase and Quadrature-Phase (I/Q) vector modulation through the use of modern photonic components and sub-systems which offer extremely wide RF intrinsic bandwidths. All-electronic vector modulators suffer from frequency coverage limitations and amplitude and phase instability due to components such as phase shifters and variable gain controllers operating at or near 100% bandwidth. In stark contrast, once an RF signal has been modulated onto an optical carrier, the percent bandwidth of the RF to carrier is typically less than 0.01% percent.

The fundamental mechanisms and basic electronic and photonic components needed to achieve vector modulation is introduced first. The primary electrical component required in most architectures is the 90° RF hybrid coupler, which is required to generate the RF I and Q terms. The two primary photonic building blocks, aside from the laser, electro-optic modulator and demodulator, are Mach-Zehnder Modulators (MZM) and Variable Optical Attenuators (VOA). Through the utilization of these components, multiple past architectures are explored and multiple new architectures are designed simulated.

For each architecture, there is a discussion on the practical implementation. Considerations such as system complexity, integration, and sensitivity to unwanted environmental stimuli are taken into account with potential solutions to alleviate these risks. In closing, the noise figure and its impact on Spur-Free Dynamic Range (SFDR) for a basic RF photonic link is derived to provide a system-level figure of merit that can be used, in most RF applications, to determine the overall performance utility current and future designs.

1 INTRODUCTION

Radio Frequency (RF) photonic processing has been a highly researched field over the past decade. The allure of using optical components for manipulating RF signals spawns from the ultra-wideband capabilities of these devices. Many traditional RF techniques such as source generation, mixing, and channelization have been implemented using optical devices. Typical telecommunication optical components operate in the spectral region around 193 THz. When an RF signal is modulated onto an optical carrier near 193 THz the percentage bandwidth of the RF to carrier is almost negligible, which translates into extremely low amplitude and phase variations over the RF bandwidth of interest. This response is in contrast to wideband electrical components which operate at, or over, 100% of their bandwidth resulting in unwanted amplitude and phase fluctuations over frequency.

Next generation ultra-wideband transmission and processing systems will rely on precise amplitude and phase control of extremely high speed signals. Digital telecommunication systems will require very fast amplitude and phase modulation and demodulation while minimizing unwanted amplitude and phase fluctuations to drastically increase information density per channel. Additionally, ultra-wideband analog systems for commercial and defense markets will require components that can control a signal's complex characteristics with a high degree of fidelity and stability. The focus of this thesis is to review multiple architectures and offer new designs, to the author's knowledge, that achieve wideband vector modulation utilizing RF photonic processing.

2 I/Q VECTOR MODULATION

The generation and control of a signal's In-phase and Quadrature (I/Q) components are required to implement (I/Q) vector modulation. (I/Q) generation is used extensively in analog and digital systems. Radar is one field that relies heavily on the ability to generate I and Q. Modern radars are coherent systems that require retention of the received signal's phase information after mixing down to baseband for processing. Without the I and Q channels, the baseband phase information of the received signal is ambiguous in two quadrants of the complex plane. This ambiguity can lead to false conclusions of a target's characteristics.

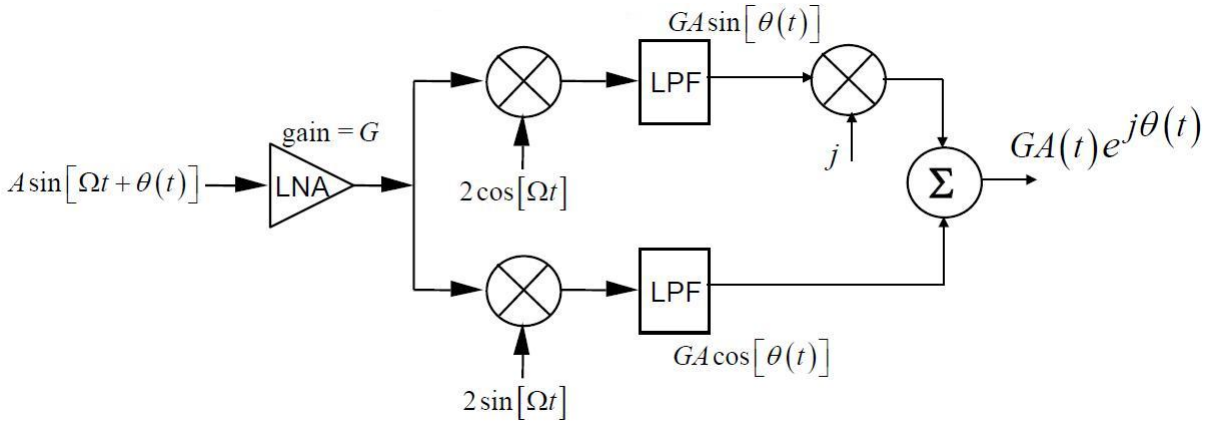

Figure 1: I/Q block diagram for radar receiver [1]

As shown in figure 1, an incoming signal is split and then mixed with the I and Q channels $2cos[\Omega t]$ and $2sin[\Omega t]$. This mixing downconverts the original signal from the frequency Ω to base band. The two signals are then lowpass filtered to reject higher frequency content. The top channel is then multiplied by j. By summing the two channels, the amplitude and phase information is retained due to Euler's formula,

$$e^{jx} = cos(x) + jsin(x) \tag{1}$$

Euler's equation also shows that if the signal flow of figure 1 is reversed, the amplitude and phase of $A(t)e^{\theta(t)}$ can be controlled by properly weighting G in each channel, which is shown

in figure 2.

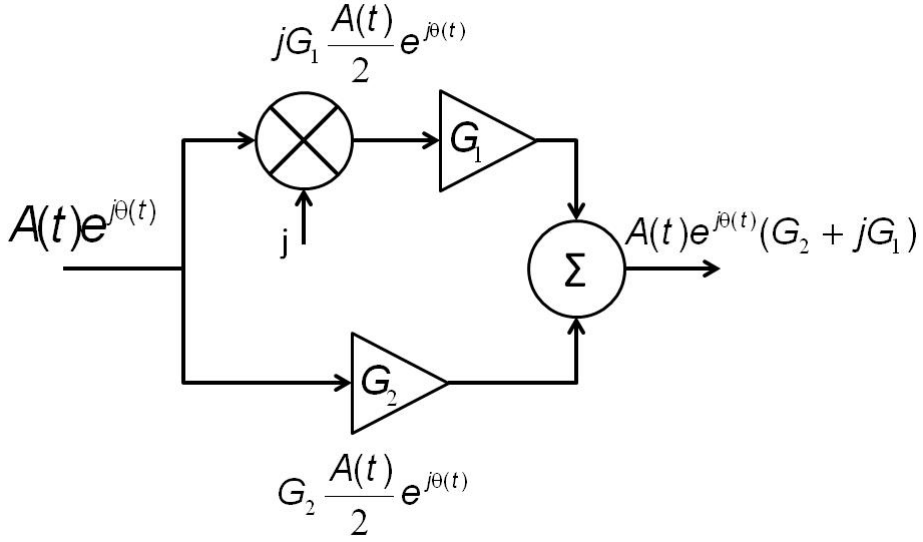

Figure 2: I/Q block diagram of mathematical operation flow.

The output of figure 2 can be written as,

$$A(t)e^{\theta(t)}(G_1 + jG_2) = A(t)e^{\theta(t)}Ce^{\varphi} \tag{2}$$

where,

$$C = \sqrt{G_1^2 + G_2^2} \tag{3}$$

$$\varphi = tan^{-1}\left[\frac{G_1}{G_2}\right] \tag{4}$$

From equation 2, it is shown that the amplitude and phase of the summed signal is dependent on the gain G_1 and G_2 resulting in a vector modulator with a phase control range of $\pi/2$. G_1 and G_2 must be set appropriately if a constant amplitude, C, is to be maintained while the phase, φ, is changed.

The equations above represent the fundamental mathematical mechanisms for I/Q vector modulation. By splitting a signal into two channels, phase shifting one channel by $\pi/2$, controlling the amplitudes of each channel, and summing the channels, the phase and amplitude of the output signal can be controlled by the amplitudes of each of the two split channels. Figure 3 depicts a simplified block diagram of the process described above.

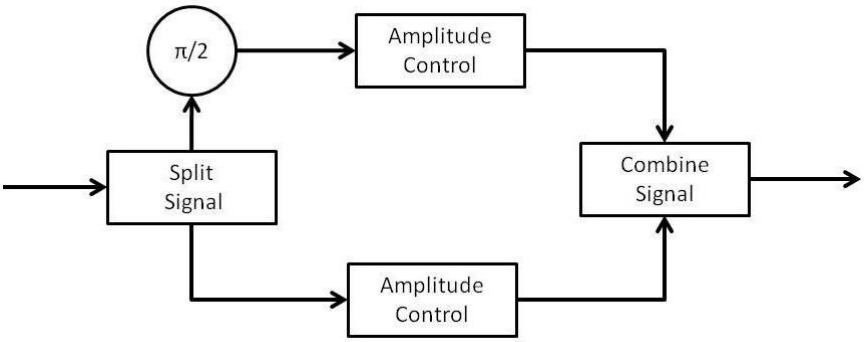

Figure 3: Block diagram of fundamental I/Q vector modulation concept.

3 ARCHITECTURE COMPONENTS

As described previously, the mechanism for phase and amplitude control of a summed signal is the amplitude of the individual channels containing I and Q. The system is an analog process which means the phase and amplitude resolution is limited by the fidelity of control and stability of the two summed channels. Figure 4 shows a block diagram of a simplified RF vector modulator with RF amplitude control in the electrical-domain.

To obtain RF amplitude control in the optical domain, the electrical signal must first be modulated onto an optical carrier. Figure 5 shows a basic RF photonic link with amplitude control. The laser is modulated with the input RF. The optical signal then enters a device that controls the amount of light transmitted. The resulting light is then detected by a photodetector which converts the RF back into an electrical signal. Figure 6 depicts the optical variation of the previous RF design for I/Q vector modulation. After the RF signal has been modulated onto an optical carrier, the signal is then optically split between two arms where amplitude control is implemented, and then detected and passed through an RF hybrid.

Both systems perform the same function but have one core difference; the optical amplitude control components have a substantial advantage in bandwidth capabilities. Practical wide-band electrical amplitude controllers operate at bandwidth percentages of 100% or above. The optical components operate at bandwidths on the order of THz, which makes the operational bandwidth to RF signals well under 0.01%. The importance of this property lies in the fact that the components using near to 100% or more of their bandwidth have problems with amplitude and phase variations over the operating bandwidth, resulting in an overall system error margin.

The 90° hybrid coupler is used to provide the necessary phase difference and summation of the two channels for I/Q operation. Phase shifting the RF by 90° is not easily obtainable in the optical domain. There is a trade off between system complexity and bandwidth when

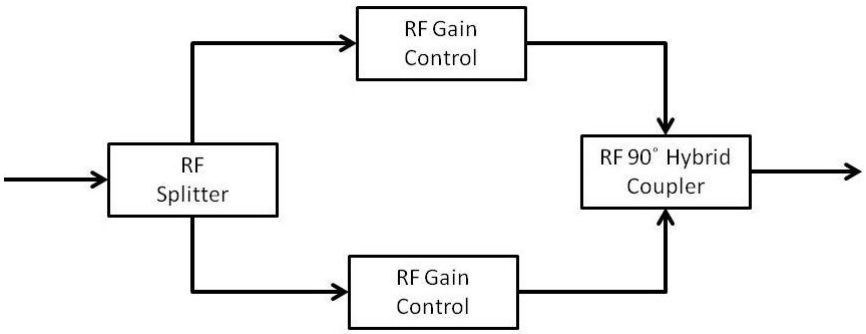

Figure 4: Block diagram of a RF I/Q vector modulator with amplitude control in electrical-domain.

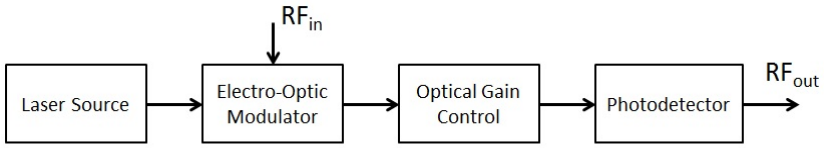

Figure 5: Block diagram of a basic RF photonic link with optical gain control.

dealing with the RF hybrid. The hybrid offers a simple coupler design but has limited bandwidth. The photonic approach has extremely wide bandwidth but at the cost of increased system complexity and cost. These aspects will be further explored. The following sections will investigate the optical amplitude control and electrical phase shifting components for the proposed architectures found in later sections.

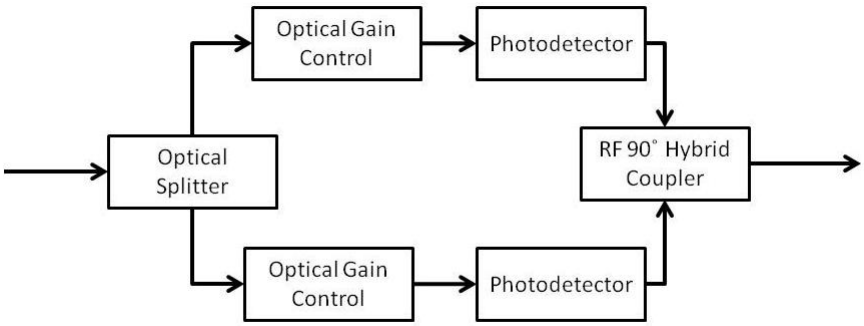

Figure 6: Block diagram of a RF photonic I/Q phase shifter with amplitude control in optical-domain.

3.1 Mach-Zehnder Modulator

A Mach-Zehnder modulator (MZM) uses the principle of interferometry to vary the optical amplitude through the device. Figure 7 depicts the basic operation of a typical MZM. The incoming light is split by an optical coupler where one or both arms phase shift the channelized light before recombining with another optical coupler. The electric field scattering matrix is defined as,

$$\begin{bmatrix} E_{out,1} \\ E_{out,2} \end{bmatrix} = \frac{1}{\sqrt{2}} \begin{bmatrix} 1 & j \\ j & 1 \end{bmatrix} \begin{bmatrix} e^{-j\theta_1} & 0 \\ 0 & e^{-j\theta_2} \end{bmatrix} \frac{1}{\sqrt{2}} \begin{bmatrix} 1 & j \\ j & 1 \end{bmatrix} \begin{bmatrix} E_{in,1} \\ E_{in,2} \end{bmatrix} \tag{5}$$

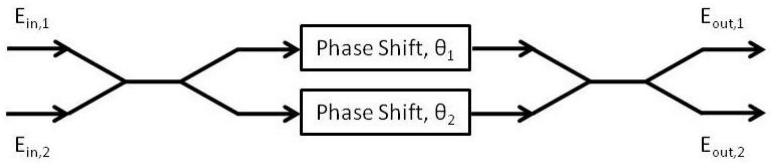

Figure 7: Block diagram of a MZM.

Common high speed optical phase shifters are made from the nonlinear material $LiNbO_3$. The couplers can also be fabricated from the same material resulting in a very compact integrated optical modulator. The process by which the optical wave is shifted in phase through $LiNbO_3$ is known as Pockels effect, where the index of refraction is changed by an applied electric field across the material given by,

$$n(E) = n_0 - \frac{1}{2} r n^3 E \tag{6}$$

n_0 is the reference refractive index, E is the electric field applied, and r is the electro-optic coefficient which is typically $10^{-12} \frac{m}{V}$. The phase of the optical wave is,

$$\theta = n(E) k_0 L \tag{7}$$

where k_0 is the wavenumber in a vacuum and L is the spatial location of the wave. Substituting equation 6 results in,

$$\theta = k_0 L(n_0 - \frac{1}{2} r n^3 E) \tag{8}$$

The electric field, E, (assumed to be a parallel plate configuration), applied across the material is given as,

$$E = -\nabla V = \frac{V}{d} \tag{9}$$

Using the fact that $k_0 = 2\pi/\lambda_0$, the optical phase shift through the $LiNbO_3$ is now,

$$\theta = \theta_0 - \frac{\pi}{\lambda_0 d} V r n^3 \tag{10}$$

where θ_0 is the inherent phase shift resulting from n_0 from equation 6. The final form of the optical phase shift equation can be written as,

$$\theta = \theta_0 - \pi \frac{V}{V_\pi} \tag{11}$$

where,

$$V_\pi = \frac{d\lambda_0}{L r n^3} \tag{12}$$

V_π is the voltage required to phase shift the optical wave by 180° with respect to the inherent phase shift θ_0, which causes either a maximum or minimum at the output of the second coupler. Because the transfer function is periodic over voltage, V_π also sets the dynamic range and noise figure of the photonic system. Suffice to say, V_π is extremely important when designing MZM devices.

The scattering matrices from equation 5 can be collapsed to,

$$\begin{bmatrix} E_{out,1} \\ E_{out,2} \end{bmatrix} = \frac{1}{2} \begin{bmatrix} E_{in,1}(e^{-j\theta_1} - e^{-j\theta_2}) + jE_{in,2}(e^{-j\theta_1} + e^{-j\theta_2}) \\ jE_{in,1}(e^{-j\theta_1} + e^{-j\theta_2}) - E_{in,2}(e^{-j\theta_1} - e^{-j\theta_2}) \end{bmatrix} \tag{13}$$

For simplicity, let the electric field amplitude entering port 2, $E_{in,2}$, equal zero and let the top output be the only output considered,

$$E_{out,1} = \frac{1}{2} E_{in,1}(e^{-j\theta_1} - e^{-j\theta_2}) \tag{14}$$

Now let,

$$\theta_1(V) = \theta_0 - \pi \frac{V}{V_\pi} \tag{15}$$

$$\theta_2 = \theta_0 \tag{16}$$

which represents the assumption that θ_1 and θ_2 both are referenced to the same inherent phase shift but only θ_1 has a variable phase shift with respect to applied voltage. Equation 14 can now be written as,

$$E_{out,1} = \frac{1}{2} E_{in,1} e^{-j\theta_0}(e^{j\pi \frac{V}{V_\pi}} - 1) \tag{17}$$

Figures 8 and 9 show the real part of $E_{out,1}$ versus the applied voltage, V, when $E_{in,1}$ and V_π are set to 1 and also when $E_{in,1}$ remains 1 and V_π is set to 2. The two plots clearly show a sine function, which is a result of the exponential properties. Because the electric field transfer function is a sine function, curved portions exist which will limit the amplitude modulation possible. The most linear section of the transfer function is typically the ideal location to vary the electric field amplitude. Most MZM devices have an RF input and bias input. The bias input is used to control what region of the transfer function the modulation will be induced. The bias has a direct impact on spur-free dynamic range (SFDR) of an RF photonic system.

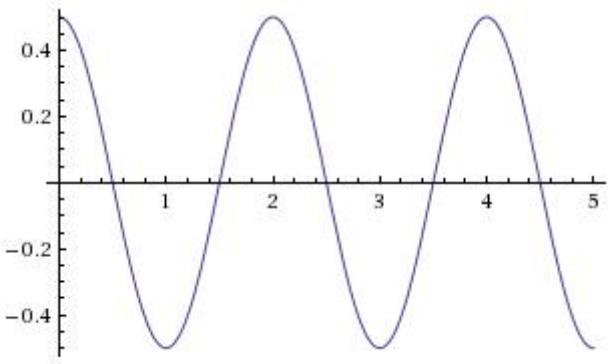

Figure 8: Magnitude of $E_{out,1}$ with $V_\pi = 1$.

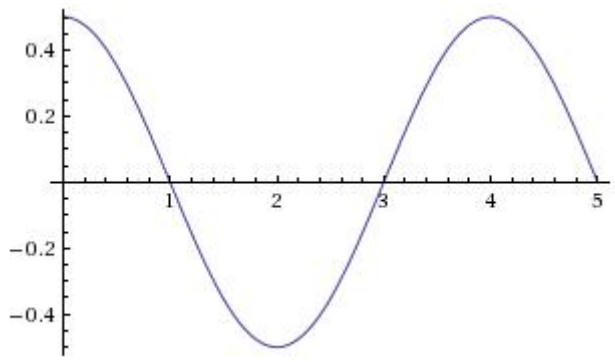

Figure 9: Magnitude of $E_{out,1}$ with $V_\pi = 2$.

Using the optical simulation tool RSoft, figures 10 and 11 show how bias selection impacts system performance. Figure 12 shows the simulation setup. A 10GHz signal is biased close to the linear region of the transfer function, and then biased away from the linear region. As shown, second and third harmonic spurs increase which is very problematic in many high performance analog systems. However, frequency comb generation is one application where multiple spurs are desired. Utilizing different bias regions and optical mixing properties of MZMs, highly predictable spurs can be generated [2]. The results of a comb technique are shown in figure 13.

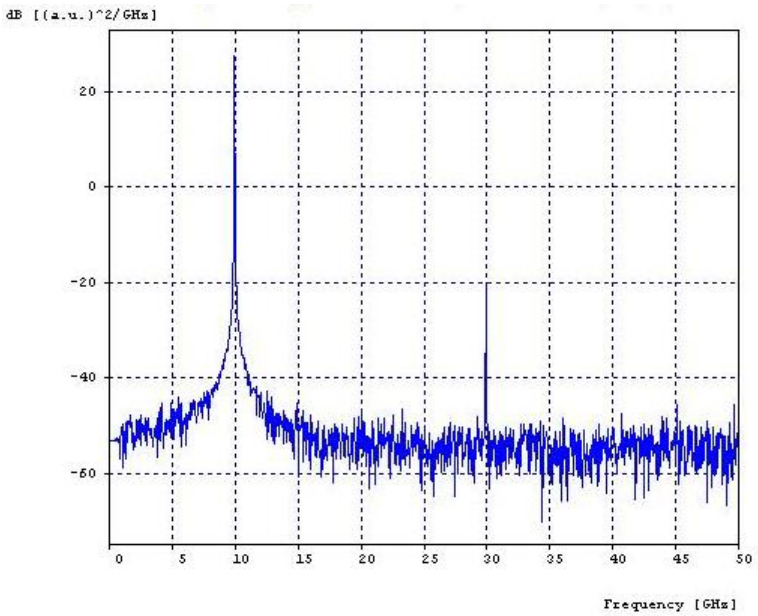

Figure 10: Gain vs. frequency when biased close to linear region.

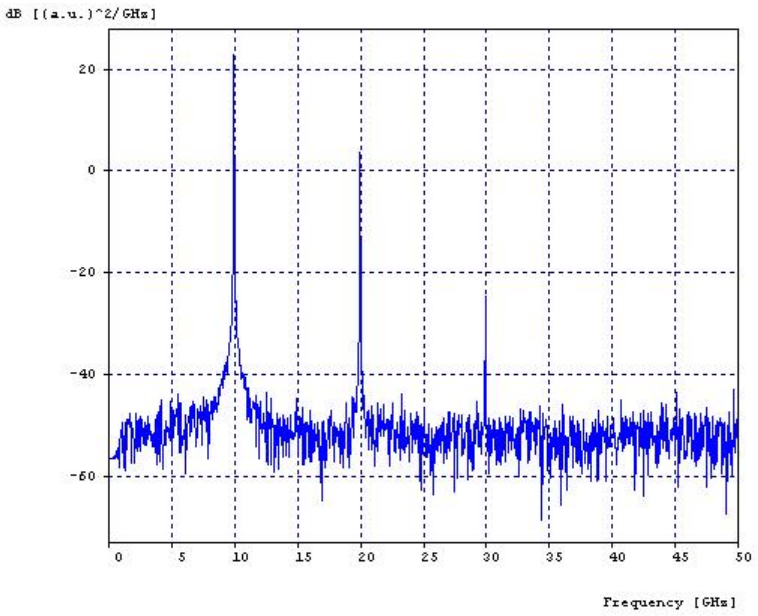

Figure 11: Gain vs. frequency when not biased close to linear region.

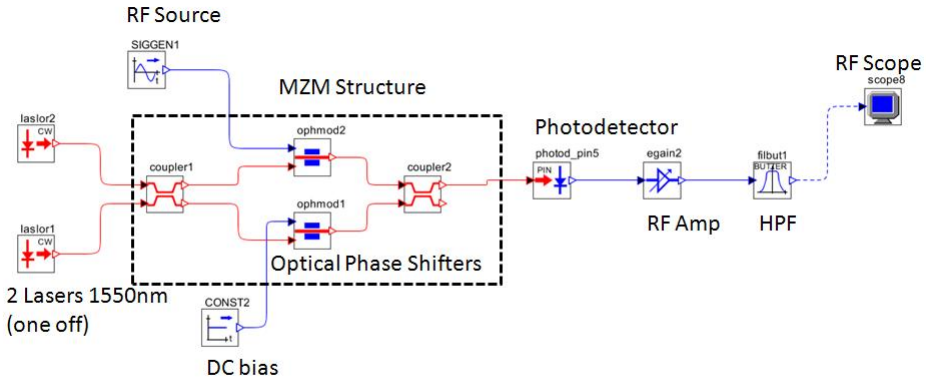

Figure 12: RSoft simulation setup for simple MZM tests.

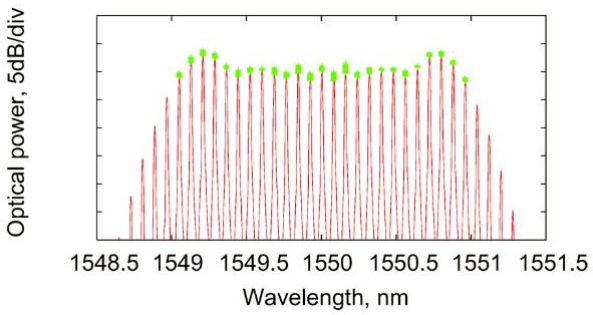

Figure 13: Optical comb generation [2].

MZMs are used for their extremely fast response to applied electric fields. Modulators with bandwidths higher than 70GHz have been demonstrated [3]. The mechanism by which I/Q phase shifting operates is based on amplitude control. Therefore, with proper design, phase shifting speeds can approach update rates on the order of picoseconds if a high speed MZM is used for amplitude control. Another key benefit of Mach-Zehnder modulators is the fact that there exists an RF phase difference of 180° between the two output ports of the second 3dB coupler shown in figure 7. This unique property will be further explored in subsequent sections.

3.2 Variable Optical Attenuators

Amplitude control is the central process for vector modulation in the architectures proposed thus far. The MZM achieves amplitude control through interferometry. Variable optical attenuators (VOAs) are also used for manipulating optical amplitude. Typical VOAs operate by either blocking or redirecting a percentage of the light passing through by using an electrical control signal. MEMs VOAs are among the most popular devices for optical amplitude control. The speed and attenuation range of the optical amplitude control devices are directly impact the performance of the overall photonic vector modulator system. The speed of the VOAs determines the update rate for phase and amplitude while the attenuation range, and jitter error, determine the resolution and phase shifting range possible. For example, if the two attenuation coefficients had only a maximum difference of $10dB$, then the maximum phase range would be 84.3°. However, with an attenuation range of $20dB$ a phase shift of 89.4° is possible.

$$\phi = tan^{-1}\left[\frac{0dB}{10dB}\right] = 84.3 \tag{18}$$

$$\phi = tan^{-1}\left[\frac{0dB}{20dB}\right] = 89.4 \tag{19}$$

Commercial off the shelf MEMs VOAs achieve update rates of 100's of nanoseconds with attenuation ranges covering greater than 30dB are readily available. Packaged MEMs VOAs also have a relatively small footprint making them very relevant for compact systems. MZM structures and VOAs are the two methods of amplitude control that will be used for exploration of multiple designs within this thesis.

3.3 90° RF Hybrid Coupler

The RF hybrid coupler is responsible for obtaining the 90° phase difference between the two channels. As discussed earlier, the benefit of optical processing of RF signals is the extremely wide bandwidth capabilities coupled with very low variations in phase and amplitude over RF range frequencies. Because the hybrid coupler is an RF (electrical domain) component, the system bandwidth and variation are limited to the coupler's characteristics.

Equation 20 gives a 90° hybrid coupler scattering matrix derived from figure 14 [4]. When designed correctly, the branch-line coupler evenly divides the RF power entering at port 1 between ports 2 and 3 while causing a 90° phase difference in the signals exiting 2 and 3. Port 4 is usually isolated, or terminated, meaning no power is coupled. It is meaningful to note the dependence on wavelength in the hybrid coupler design shown in figure 14. This has a direct impact on the operational bandwidth of the coupler. Without the use of cascaded sections of differing wavelengths, the bandwidth is limited to about 10% to 20% [4].

$$\left[S \right] = \frac{-1}{\sqrt{2}} \begin{bmatrix} 0 & j & 1 & 0 \\ j & 0 & 0 & 1 \\ 1 & 0 & 0 & j \\ 0 & 1 & j & 0 \end{bmatrix} \tag{20}$$

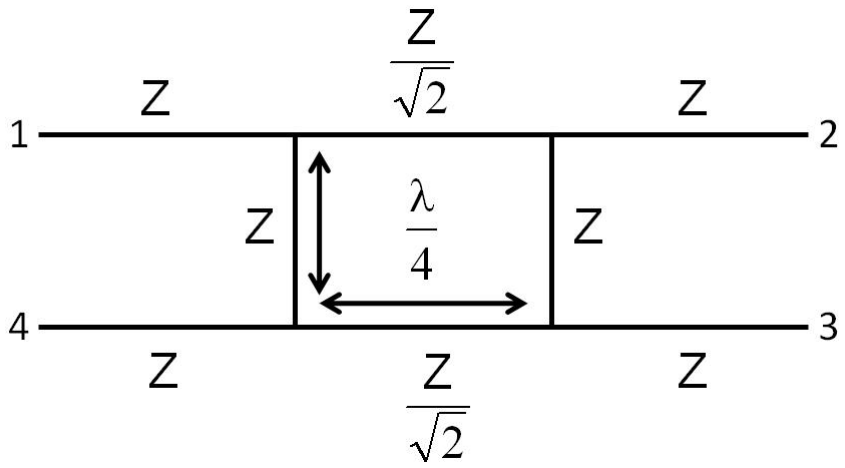

Figure 14: Branch-line coupler for 90° hybrid.

3.4 90° Alternatives

3.4.1 RF Circuit Design

There exist other designs for obtaining the required 90° phase difference that have the potential to improve the bandwidth and variation. One alternative consists of microstrip radial stubs to induce a broadband phase shift [5]. The circuit typically attempts to act as an all-pass filter that causes a flat phase shift over a range of frequencies. However, as with the hybrid coupler, making an RF phase shifter circuit that remains flat over frequency is not trivial. Figure 15 shows the design and photograph of a 1-22GHz MMIC Phase Shifter and figure 16 shows the amplitude and phase variations. The gain variation over all phase states appears to be in the range of about $1dB$ while the phase error error at 90° appears to be about 3° over frequency.

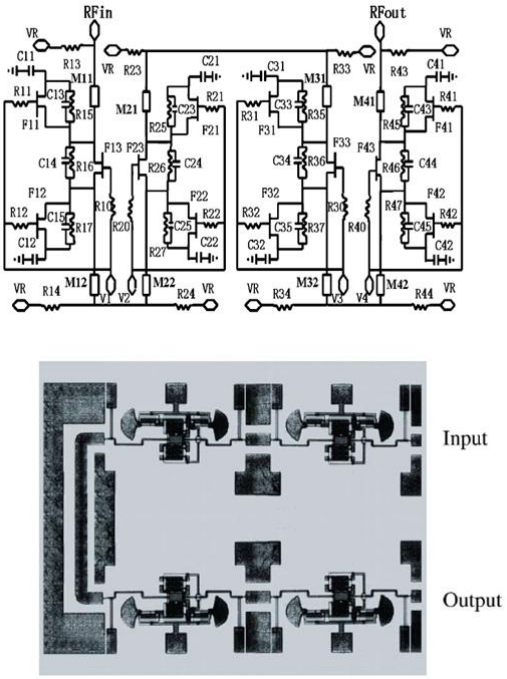

Figure 15: 1-22GHz MMIC Phase Shifter [5]

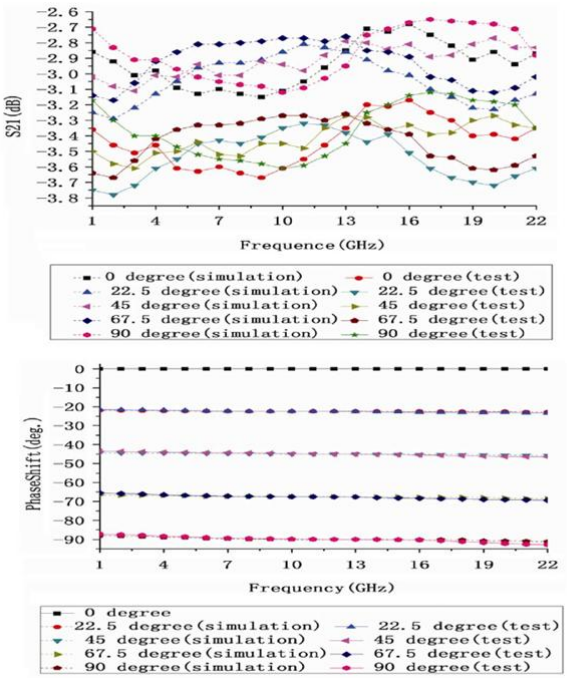

Figure 16: Amplitude and phase variation of 1-22GHz MMIC Phase Shifter [5]

3.4.2 Optical Carrier Suppressed Single Side Band (CS-SSB)

The hybrid coupler and RF phase shifter both suffer bandwidth limitations and amplitude and phase variations due to the devices operating near or over 100% of their respective bandwidths. Another possible solution is to handle the RF 90° phase shift in the optical domain. An optical 3dB coupler causes a phase difference of 90° between the two output ports. This optical phase difference does not translate to an RF phase difference because the optical carrier and sidebands are both phase shifted equally resulting in no overall RF phase shift when the signals beat at the photodetector. However, if either the carrier or sideband's phase was held constant while the other's changed, the RF phase would be shifted by that amount when mixed at the photodetector. This process will be further explored in subsequent sections.

4 PREVIOUS RF PHOTONIC I/Q DESIGNS

This section will present RF photonic designs that provide insight into the different techniques used to achieve vector modulation. Many papers and designs focus on phase shifting the RF, thus calling their systems RF photonic phase shifters and not RF photonic vector modulators. In most cases it is assumed that amplitude control can be easily implemented into the phase shifting system, creating a vector modulator. Because of the close relationship between phase shifters and vector modulators, the two terms will be used interchangeably. Potential designs, found in section 5, will show connections to the designs of this section.

4.1 Switch Network with RF Hybrid

The first RF photonic phase shifter will utilize the most basic configuration of I/Q generation and control. Figure 17 recalls the basic photonic block diagram presented earlier. As previously discussed, the optical signal carrying the RF information is split into two channels where amplitude control is induced through any number of optical amplitude controlling devices. The signals are converted back to the electrical domain via photodetectors/photoreceivers and then combined with an RF hybrid coupler causing the necessary 90° phase difference between the two channels. This design only obtains a control range of 90°. The design described below will introduce a process to increase the phase shifting range to 360° using a network of switches and by profiting from the 180° properties of dual port MZM devices.

4.1.1 Theory and Design

Figure 18 shows the block diagram given in the paper by Erwin H.W. Chan and Robert A. Minasian [6]. The laser source provides the necessary optical carrier, while the MZM electro-optically modulates the RF signal, $V_{RF}(t)$, onto the optical carrier. V_{bias} is the voltage used to set the MZM to its most linear region. The two $3dB$ couplers and switches are used to select

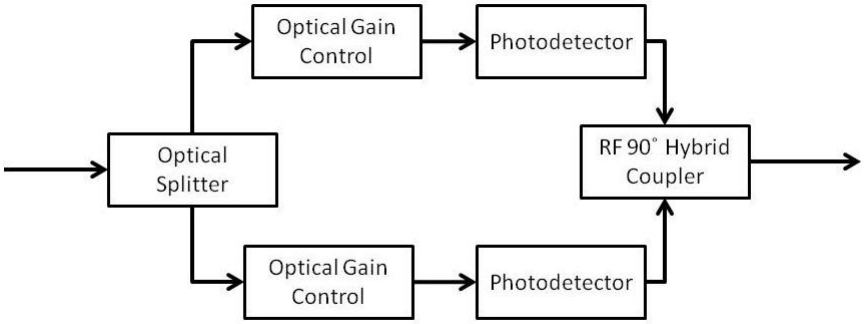

Figure 17: Block diagram of a RF photonic I/Q phase shifter with amplitude control in optical-domain.

the quadrants to obtain the full 360° of phase shift. The VOAs are used for amplitude control of the two RF signals combined at the 90° hybrid coupler.

A dual port MZM is used to obtain a 180° RF phase shift between the two optical output ports. This result is apparent when examining the MZM scattering equation below. Utilizing this fact of MZM operation, two switches and two $3dB$ couplers are used to select whether the inputs to the hybrid coupler are either 0°/0°, 0°/180°, 180°/0°, or 180°/180° corresponding to selection of the four quadrants. Figure 19 shows the diagram used in the paper to describe how the switches are operated for full a 360° phase range. The a and b ratio refers to the amplitude ratio between the two arms entering the hybrid coupler. Equation 22 shows the dependence of amplitude ratio on phase of the combined signal.

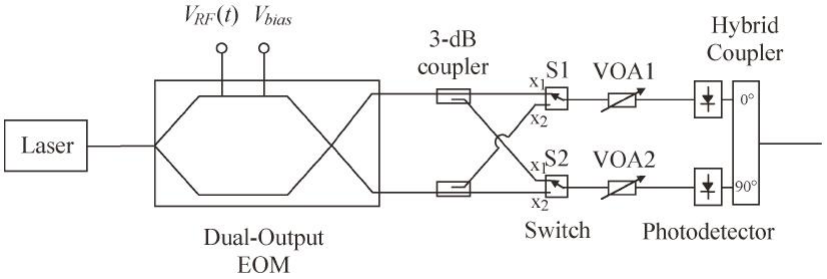

Figure 18: Block diagram of a RF photonic I/Q phase shifter using switch network and dual port MZM [6].

$$\begin{bmatrix} E_{out,1} \\ E_{out,2} \end{bmatrix} = \frac{1}{\sqrt{2}} \begin{bmatrix} 1 & j \\ j & 1 \end{bmatrix} \begin{bmatrix} e^{-j\theta_1} & 0 \\ 0 & e^{-j\theta_2} \end{bmatrix} \frac{1}{\sqrt{2}} \begin{bmatrix} 1 & j \\ j & 1 \end{bmatrix} \begin{bmatrix} E_{in,1} \\ E_{in,2} \end{bmatrix} \tag{21}$$

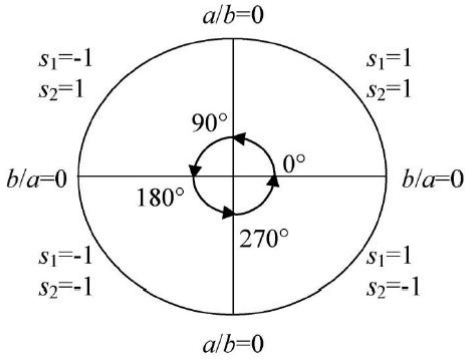

Figure 19: Diagram of switch quadrant selection [6].

$$\phi = tan^{-1}\left[\frac{b}{a}\right] \tag{22}$$

4.1.2 Results and Discussion

Figure 20 shows the simulated and experimental results obtained by the group using an 100MHz signal. The simulation and experimental products are in very good agreement across the full range. Recall the equation below,

$$C = \sqrt{a^2 + b^2} \tag{23}$$

The group was concerned with holding the amplitude, C, constant while moving the phase. This was accomplished by selecting values which held C to a ratio of 1 while stepping through the 360°. The group obtained a $0.2dB$ variation over the entire phase range. Recall that the earlier RF circuit design had an amplitude variation of about $1dB$ [5]. However, the RF circuit was designed and tested at much higher frequencies than the photonic system under discussion. It will be shown in later sections that this photonic approach is still superior in gain variation even at much higher frequencies.

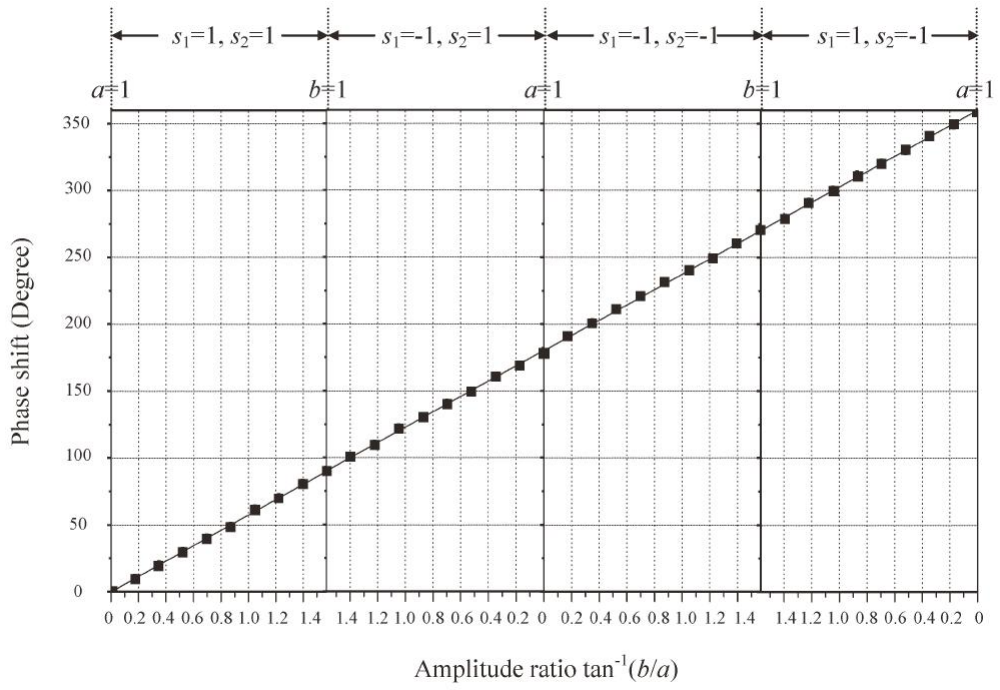

Figure 20: Results of switch network RF photonic phase shifter at 100MHz [6].

This photonic switch network approach is very appealing due to its simplicity. The system's update rate is limited by the VOAs, which are approaching nanosecond speeds in commercial products. The optical switch speed is also a consideration; however, nanosecond optical switches are commercially available. Because the system is entirely analog, control and resolution is dictated by the electronic control of the VOAs and switches.

The two biggest limitations in this design are RF hybrid coupler characteristics and the length matching required for all paths. As shown before, hybrid couplers have bandwidth limitations and phase and amplitude variation difficulties. The $1 - 22GHz$ RF circuit could be used to generate the 90° phase difference in one arm and then combined using a broadband RF coupler. If the RF circuit were designed to only shift the signal by 90° instead of the multiple stages described, more attention could be paid to phase and amplitude variation over frequency for the single desired phase shift. Using this optimized circuit design would potentially improve variations over frequency. Current commercial optical components would also cause the system to be much larger than many applications desire. However, the rapidly

growing field of integrated photonics has already realized all the components described above at the chip level [7].

Length matching is very important because a true time delay difference between paths will cause a periodic interference pattern with nulls at frequencies where the time delay corresponds to a 180° phase difference between paths. While this may not be of importance for narrowband systems, it can be a non-trivial problem for wideband operation.

There are multiple solutions to obtain the highly accurate length matching necessary for wideband operation. The simplest way is through coarse fiber length matching and then to use a fiber line stretcher for fine tuning. A pulse generator and oscilloscope can be used to tune the leading edges of the two resulting pulses. A network analyzer can also be used to tune the lengths. Viewing the gain over frequency will show the interference pattern of the coupled signals. By tuning the fiber stretcher, the pattern will change. The gain over frequency will be flat, or maintain the intrinsic transfer function of the system, when the two arms are very closely matched.

Another solution to match the two paths is with a wideband RF variable true time delay. Figure 21 shows time delay versus applied voltage for a commercial Hittite chip that can achieve a true time delay of up to 70 picoseconds in the frequency range of DC-24GHz. The chip would need to be inserted after the photodetectors and before the 90° hybrid. Also, having a chip in both arms, instead of only one, would keep the gain and variations between the arms more consistent and would allow more flexibility when searching for the correct tuning.

Optical ring resonators offer tunable true-time delay in a very compact size. Ring resonators have gained much interest in the photonics community over the past decade. These devices act as all-pass filters with an overall group delay. The group delay is frequency dependent. The spectral response of the ring resonator is determined by the inverse of the round trip of the ring's overall delay caused by the ring's radius. This spectral response is bell shaped and

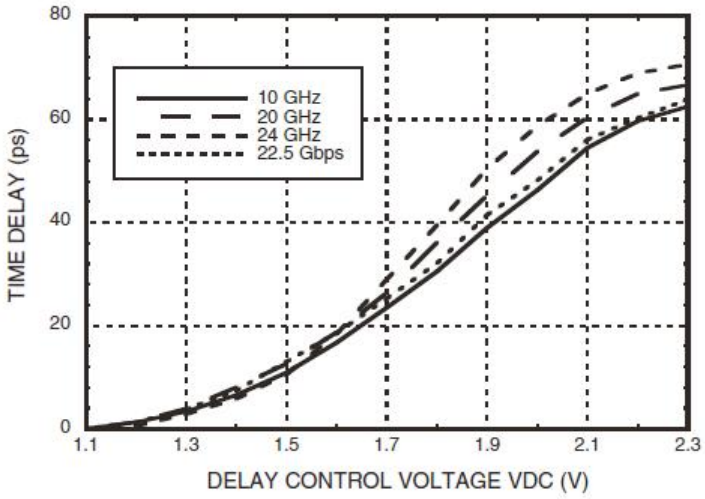

Figure 21: Time delay versus applied voltage of Hittite HMC910LC4B broadband analog time delay DC-24GHz.

requires cascaded resonators of varying round trips to cause a flatter overall group delay for a wider range of optical frequencies. Figure 22 shows the optical resonator structure and group delay versus frequency [8].

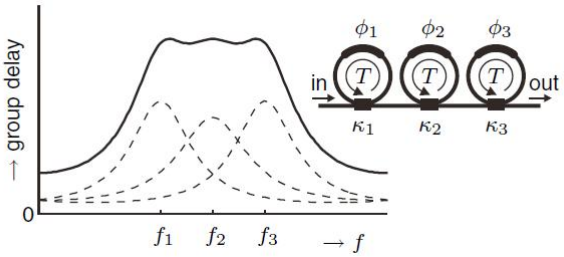

Figure 22: Ring Resonator concept for flat group delay over selected frequencies [8].

Again, the switch network design is very appealing due to the relatively simple architecture. Phase and amplitude are controlled through optical attenuators and quadrant selective through optical switches. All of these devices can be integrated onto a photonic chip. The phase resolution is dependent by the RF hybrid coupler and by the electronic control of the VOAs. Length matching all the arms has a dramatic effect on the photonic system's bandwidth and phase range. Multiple solutions for length matching were discussed and show much promise. However, as photonic chip integration becomes more precise, highly accurate length matching can be achieved in fabrication voiding the necessity for alternative length matching techniques.

The next section will discuss an approach that also utilizes an RF hybrid but its position in the system will change.

4.2 RF Hybrid with Two MZMs

4.2.1 Theory and Design

In the last section the 90° RF hybrid was used at the output of two channelized photodetectors. The next approach shifts the RF hybrid before the electro-optic conversion at the MZM. This method creates the I/Q channels before the optical components, whereas the previous method created them after. Figure 23 shows the diagram of the system under discussion [9]. This system uses two light source inputs of either differing wavelength or the same wavelength but incoherent because the two sources are coupled into the same photodetector. If both light sources were coherent then unwanted phase and amplitude noise would appear in the output RF. Also, if the wavelength difference between the light sources isn't spaced sufficiently large, unwanted spurs will arise in the bandwidth of interest.

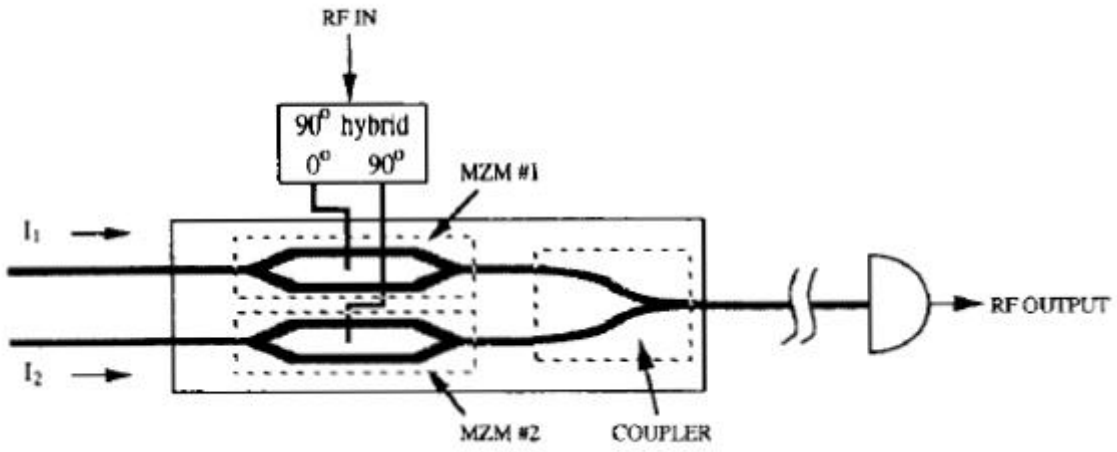

Figure 23: photonic I/Q Vector Modulator utilizing two MZMs [9].

The system in figure 23 has the same process of I/Q phase shifting through amplitude control of two channels as discussed previously. In the previous system amplitude control was accomplished through variable optical attenuators. This system varies the lasers' output powers to obtain the desired summed amplitude ratio for correct phase shift. In practice,

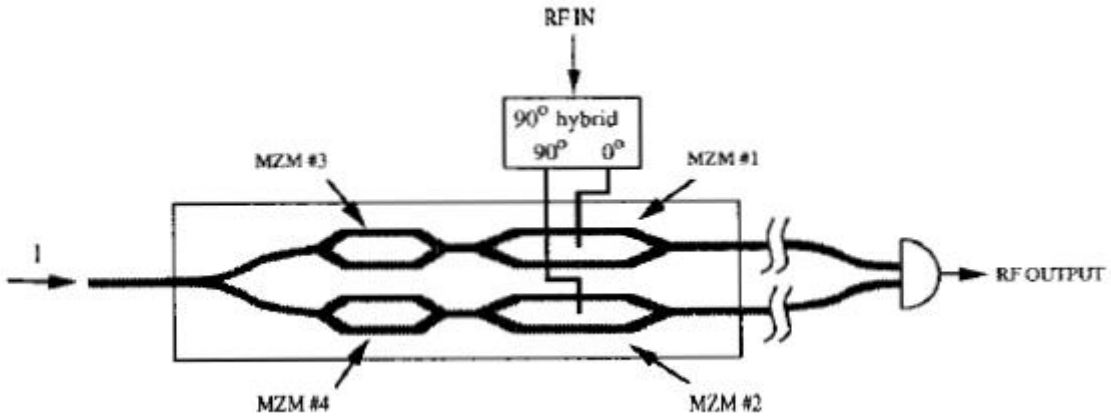

Figure 24: Photonic I/Q Vector Modulator utilizing four MZMs [9].

variable attenuators could be used in each laser path before entering the MZM architecture. Or, varying the current driving each laser could be used for the same function. The VOA approach may provide better results than current control of the lasers. This is because VOAs do not alter the wavelength or linewidth of an optical carrier. However, unless the laser has been specifically engineered for wavelength and linewidth stability under current modulation, undesired results in the output RF may occur such as increased phase noise.

Figure 24 shows a second system designed by the same group. This system requires only one light source but the addition of two more MZMs along with a photodetector that separately detects the two coherent channels. The photodetector in this system does not mix the two optical signals like a coupler would, which means coherent mixing is not an issue. The input optical carrier is split and fed into two MZMs which are used for amplitude control of the I/Q channels. These two carrier channels are then modulated with the RF signal with another set of MZMs at a 90° RF phase difference. This section of the system is the same process as the system in figure 23. Once the signals are combined at the separately detected photodetector, the RF signal can be phase shifted over a range of 90° by changing the amplitudes in the first stage of MZMs. For full 360° range of phase shift, the MZM property of 180° bi-phase operation is utilized like the switch network system described previously. By applying the

correct combination of 0° and 180° phase shifts on the top and bottom MZMs for quadrant selection, a full 360° phase shift can be obtained.

4.2.2 Results and Discussion

The experimental results obtained in this paper agree very well with the theory discussed in previous sections. The notion that phase and amplitude variation over different I/Q settings is very small relative to strictly using using RF components is verified through experimentation. The following results were obtained using the first of the two designs described in the previous section. The experiment used two $1.3\mu m$ multimode lasers that were incoherent with one another, a $3GHz$ MZM, and a $10GHz$ photodetector. The tests used a $2GHz$ input signal and a microwave network analyzer to measure phase and amplitude. Figure 25 depicts the phase error results, which shows an error of less than 1° over a 90° range. Most high-end commercial RF phase shifters are specified at a phase error of 10°, as shown in figure 26.

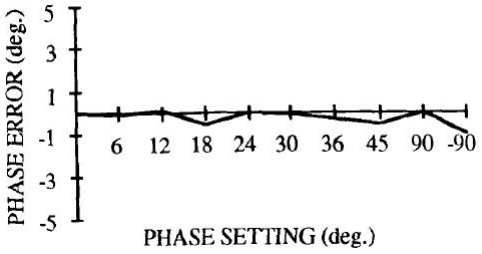

Figure 25: Phase error over different phase settings.

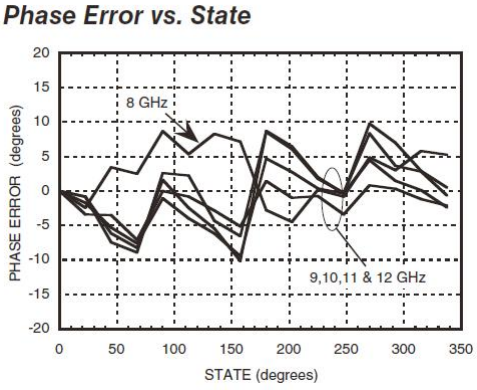

Figure 26: Data sheet screen shot of commercially available Hittite Wideband RF phase shifter phase error.

Figure 27 shows the phase change over an RF attenuation range of $30dB$. The phase modulation due to amplitude modulation is a very common undesirable result in RF attenuators. If a system requires the phase to remain the same over an attenuation range, such as in an active cancellation system where the phase difference of 180° must be maintained, variations in phase can either seriously degrade the system's functionality or require calibration look-up tables for each attenuation value set. Calibration tables can add a huge processing burden especially if there are multiple vector modulators in the system. Also, because each vector modulator will have to be specifically characterized and calibrated, manufacturing costs and time will significantly increase.

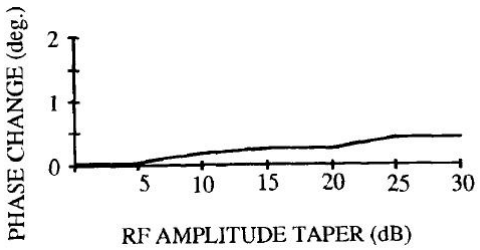

Figure 27: Phase change over RF attenuation by optical attenuation weighting.

The two RF photonic phase shifters described in this section have many of the same benefits and difficulties of the switch network system described earlier. The similar benefits are the integration potential and the amplitude control of the I/Q channels remaining in the optical domain, making the phase and amplitude variation over frequency extremely low. The first design uses control of the laser's output optical power to set the I/Q channels' amplitude. The paper shows the two lasers being separated from the MZM chip. This is because the MZM in this paper was made of $LiNbO_3$. In recent years much work has been put into fabrications that have lasers and MZMs integrated on the same chip [10]. Taking this integration one step further, photodetectors could also be integrated with the lasers and MZMs to have both RF photonic phase shifter designs each fabricated on one chip. This approach using InP can also be used for the switch network by using MZM structures instead of VOAs and switches for I/Q

channel control and quadrant selection. As discussed earlier, integration of all sections of the device is a huge benefit due to the fact that highly precise length matching between the I/Q channels is required especially for higher frequencies.

The most obvious difference in the MZM structure designs and the switch network design is that the RF hybrid coupler that creates the I/Q channels is inserted at different locations in the architectures. The switch network has the I/Q generation after the photodetectors while the MZM designs have the I/Q generation preceding the electro-optic conversion provided by the MZMs. The system performance difference between the two approaches is dependent on the electrical matching of either the photodetectors or the MZMs to the RF hybrids. System performance will be degraded, or calibration required, if the responsivity and linearity differ in the photodetectors. The quantum noise added and dark current can have an effect, but only need be taken into account if extremely resolute phase shifting is required. For most applications, quantum noise and dark current differences can be ignored especially if the photodetectors are fabricated on the same substrate.

The MZMs also must be closely electrically matched for precise phase shifting. Maintaining correct biasing of both MZMs to their most linear region is an additional difficulty. The MZM designs also require length matching between the arms that transmit the RF information. All lengths without the RF, such as the lengths between the laser and the MZM structures, are not required to be matched for the system to function correctly. Therefore, the lengths between the RF hybrid-MZM interface and the MZM-photodetector interface must be matched. As discussed earlier, RF variable true time delays can be used to match the two RF/optical arms or optical ring resonators/optical variable delay lines. Because the MZM designs are already highly integrated, length matching is less strenuous unless high frequencies are required. The next design requires no length matching because it does not achieve phase shifting through I/Q generation.

4.3 Carrier Suppressed Single Sideband

To this point the previous designs have all relied on I/Q generation and amplitude control to obtain the desired phase shift and resulting amplitude of the output RF signal. This design relies on optical phase shifting that results in an RF phase shift. The topic of this thesis is I/Q vector modulation, which is not the operation of the following design. However, it will become apparent in the potential design section where this process can be used for the I/Q method.

4.3.1 Theory and Design

As briefly discussed in previous sections, an optical phase shifter does not cause an RF phase shift. This is because the optical phase shifter operates on nanometer wavelengths and not millimeter to meter wavelengths. However, if the phase of the optical carrier and electro-optically mixed RF information is offset, the output RF signal will be phase shifted by the offset when optical-to-electrical conversion is induced at the final photodetector stage. This process relies on the ability to separate the optical carrier from the RF modulated sideband, which can be difficult if the RF is not high frequency. If the RF is about $10GHz$, commercially available optical filters can separate the carrier and sideband with relative ease. Even if the laser's frequency varies as much as $5GHz$, the passband of the optical filters can be made wide enough to tolerate such instability. However, if the optical spectrum had an RF sideband near or below $5GHz$ and the passband was the same as before, the system would loose RF phase shifting functionality.

The system described below uses carrier suppressed single sideband modulation techniques to achieve separation without the use of optical filtering [11]. Figure 28 shows the design used by the group. The optical carrier is divided through multiple stages to obtain the desired result. The top most stage provides the electro-optical modulation of the RF using two optical phase shifters in an MZM architecture. By phase modulating both arms at a phase difference of 90°, a single sideband of RF information with the optical carrier results when the two arms are joined

in the optical coupler. The bottom arm of the design labelled "Optical Phase Modulator" is used to phase shift the split optical input. Now the optical carrier output from the "Optical SSB Modulator" and the output of the "Optical Phase Modulator" can be set to differing phases. When the two signals are mixed together at a photodetector, an RF phase shift dependent on the phase difference of the two modulator sections will result.

While this architecture does produce an RF phase shift, the mixing properties of the two carriers will cause undesirable power fluctuations and nonlinear phase shifting over the control voltage range. The power fluctuations over applied voltage are a result that this device operates as an interferometric modulator. If no RF signal were input to the top section, the device would operate like a typical MZM structure. The interferometric properties of combining the top and bottom sections of the device results in a power fluctuation equal to the extinction ratio inherent of the device, which is about $15dB$ in RF power in this paper. Obviously, an RF power variation of $15dB$ over the total phase range renders this device extremely limited for practical systems requiring amplitude stability while phase shifting. To mitigate this problem the group inserted a third arm into the MZM structure.

The "DC Balance" in figure 28 is used to tune the optical phase so that the optical carrier is cancelled, or greatly attenuated, when the output of the "DC Balance" section and the "Optical SSB Modulator" section are coupled. If the optical carriers are sufficiently cancelled, the combination of the two sections results in a carrier suppressed single sideband modulation. By using this process of optical carrier cancellation, the coupling of the signal with the bottom section will not have the interferometric properties as before. Using the "DC Balance" allows phase shifting without the undesired power fluctuations. Figures 29 and 30 show the phase and RF power versus the control voltage of the "Optical Phase Modulator" section. Both figures show three plots representing the device operation without the "DC Balance" arm, with the arm set for a splitting ratio of $\alpha = 1$, and when the splitting ratio $\alpha = J_0(\Delta)/\sqrt{2}$ where

$\Delta = \pi V_{RF}/V_{\pi}$. The splitting ratio α is derived in the paper from the square-law of the resulting photo-current produced at the photodetector after the MZM device, which is why the Bessel function $J_0(\Delta)$ is present in the optimized setting for α. After optimizing for constant amplitude while controlling a predictable linear RF phase shift, the group obtained an architecture very suitable for practical applications.

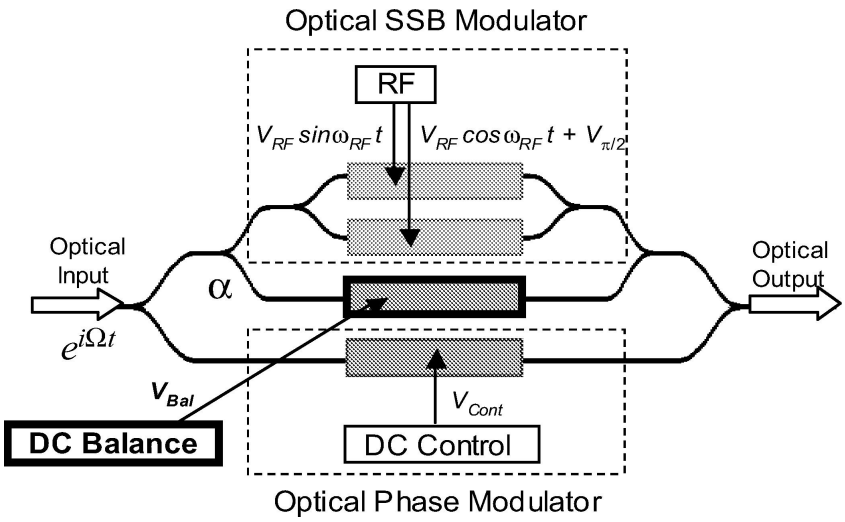

Figure 28: RF phase shifter design using optical carrier suppressed single sideband modulation [11].

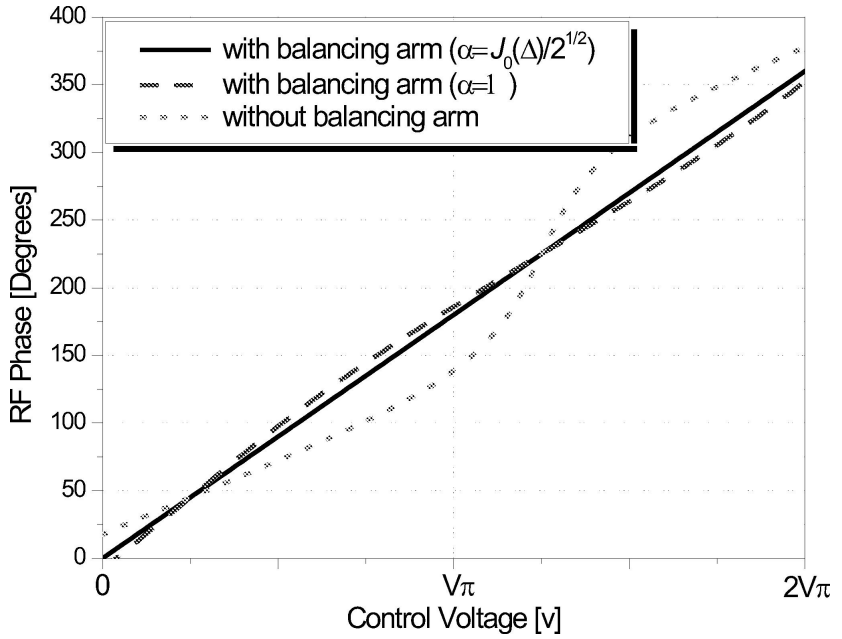

Figure 29: RF phase vs. control voltage of "Optical Phase Modulator" section [11].

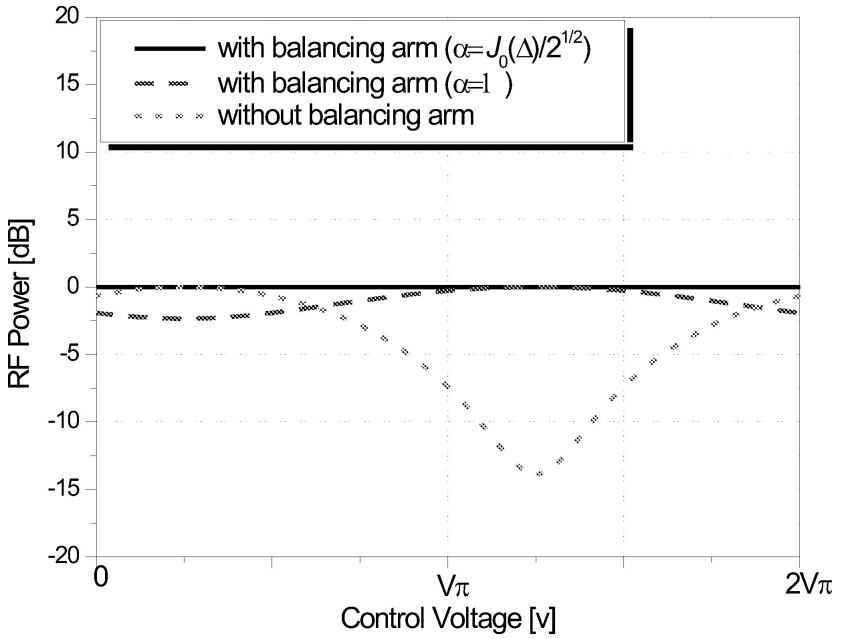

Figure 30: RF power vs. control voltage of "Optical Phase Modulator" section [11].

4.3.2 Results and Discussion

The device was fabricated to demonstrate its use in a practical application, namely a phased array architecture. Figure 31 shows the schematic of the 4-port device and the fabricated waveguide structure. For simplicity of design, the splitting ratio α was set to 1, which figure 30 shows will induce an RF power change of about $4dB$ over the full phase shift range.

Figure 32 and figure 33 show the resulting phase shift and power variation over a bias voltage of V_π. The system was setup for a triangle wave spanning $50ms$. The triangle voltage ramped up and down between $-V_\pi$ and $+V_\pi$. As was predicted by the group, the phase shift range achieves 360° while the power variation is about $4dB$.

The design described in this section is very appealing due to the highly integrated and compact package. The bandwidth of the optical sections are again extremely wideband with physical limitations not impeding until frequencies well beyond $100GHz$. However, the structure described uses and RF hybrid to obtain the correct optical mixing required for device operation. Therefore the system is limited by the bandwidth and stability of the RF hybrid. A common theme in all the designs described thus far, is the limitation of a system requiring

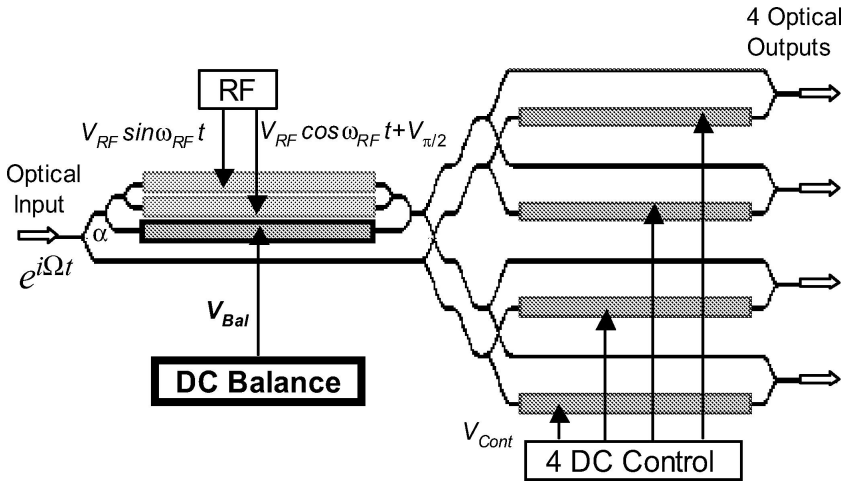

Figure 31: 4-port optical RF phase shifter array [11].

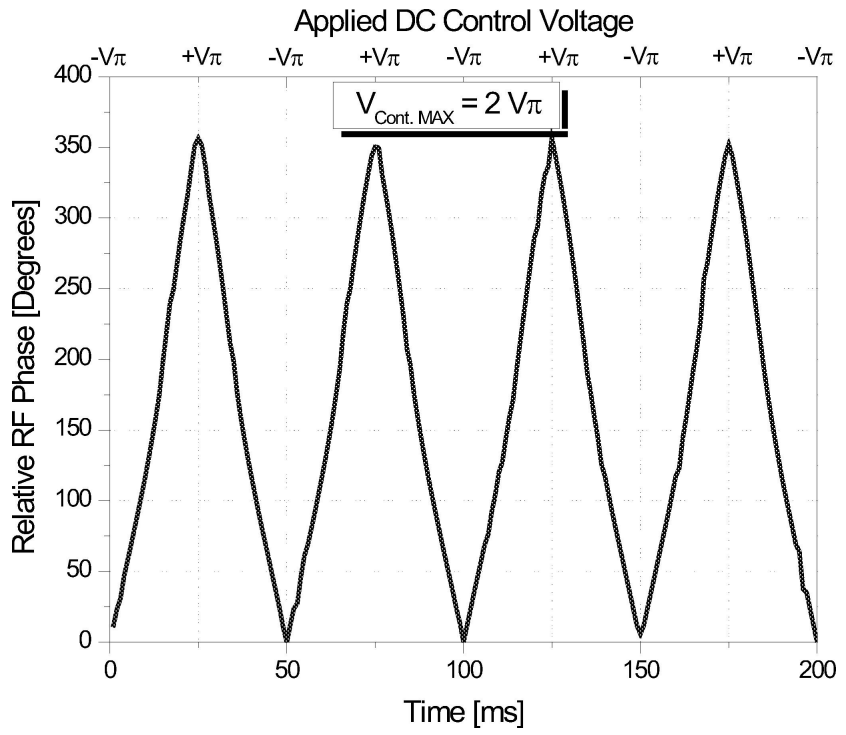

Figure 32: Measured phase results from one output port [11].

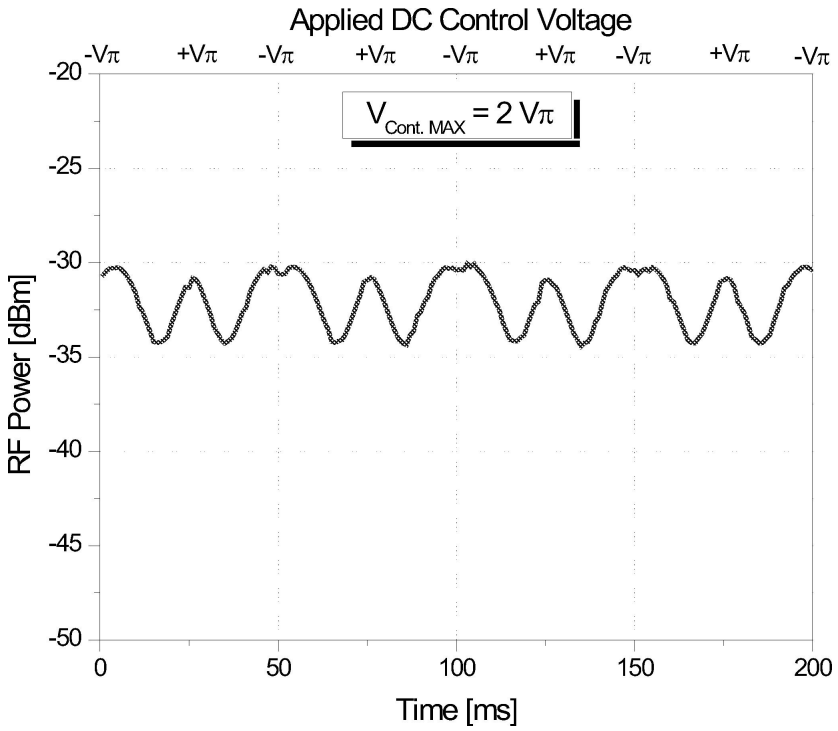

Figure 33: Measured power results from one output port [11].

RF components. One potential design will be explored in future sections that hopes to achieve an all optically generated RF phase shift where the bandwidth limitations reside only within optical or electro-optical components.

5 POTENTIAL RF PHOTONIC I/Q DESIGNS AND SIMULATIONS

This section concentrates on potential RF photonic I/Q designs. The designs proposed are considered novel to the author's knowledge. The sections leading up to this portion have laid the fundamental mechanisms by which these designs function. Each section will include a design, simulation, and discussion subsection. Each design section will recall and reiterate the processes discussed in previous sections to refresh the information needed to understand the system's functionality. Simulations will then be presented and interpreted. Finally, discussions of the pros and cons will conclude each section.

All the following simulations will use RSoft. This simulation software is used throughout many laboratories and was recommended by Professor Stephen E. Ralph of Georgia Tech for close agreement of experimental and simulation data. The main focus of the simulations in this section is phase and amplitude control, not link budget or noise figure. Noise figure will be discussed in subsequent sections. This thesis focuses on novel ways of using current devices as a system. Thus the figures of merit for these simulations will rely solely on design complexity and vector modulation.

5.1 Basic Two VOAs and Quadrant Selection

The next two sections propose architectures very similar to the switched network hybrid design described in section 4.1. The proposed designs differ in that they use an RF component for switching quadrants instead of the optical switching network. The designs are meant to decrease system complexity with the trade-off of bandwidth and gain flatness over frequency due to the RF component insertion.

5.1.1 Design

Two designs using two VOAs and an RF quadrant selector will be shown. The first design, depicted in figure 34, uses two optically split channels with VOA amplitude control for phase modulation between 0° and 90°. This process is exactly the same process used in section 4.1. The difference is the RF phase shifter at the output of the RF hybrid.

The quadrant RF phase shifter is used to select 0°, 90°, 180°, or 270°. This function serves the same purpose as the switching network discussed earlier. Figure 35 recalls the phase plot where quadrant selection is determined by the switch weightings of either 0 or 1. In the design proposed, a wideband 2-bit digital RF phase shifter can be used in place of the switching network. Section 3.4.1 showed that wideband RF phase shifters have been made with relatively small gain variation over frequency.

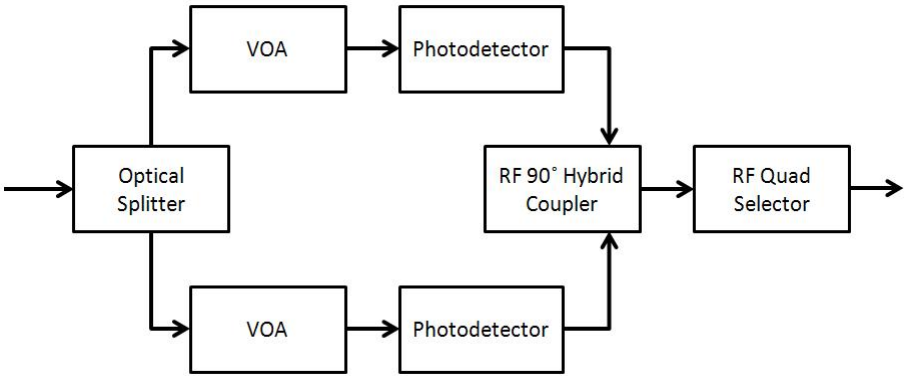

Figure 34: Block diagram of a proposed RF photonic I/Q vector modulator using two VOAs and an RF quadrant selector.

5.1.2 Simulation

Figure 36 shows the component arrangement of the RSoft simulation (the dashed boxes and labels have been included for ease of understanding). A $10GHz$ RF signal is modulated onto an optical carrier provided by the laser source. Notice the MZM structure has been manually constructed using couplers and optical phase shifters. While RSoft does provide generic MZM components, the author chose to manually create the MZM to investigate dual optical inputs,

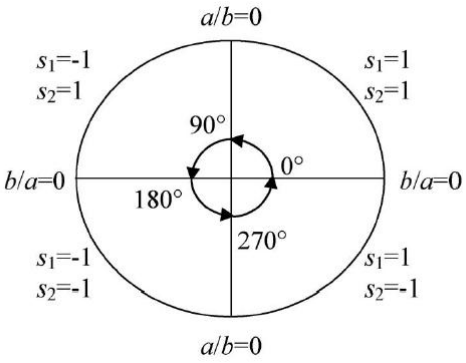

Figure 35: Diagram of switch quadrant selection [6].

optical outputs, dual RF inputs, and unbalanced optical phase shifter architectures.

After the MZM, the optical signal is then split between the vector modulator portion of the design and a reference channel. The upper signal, which will be vector modulated, is split between two VOAs for amplitude control and then converted back to RF via two photodetectors. RSoft does not contain an RF 90° hybrid. Because of this, the output of a photodetector has an RF phase shifter set to 90° and is electrically combined with the output of the other photodetector to simulate an RF hybrid coupler. The combined signal is then sent through the quadrant selector and a filter. The filter was used to block DC so that the voltage offset off all signals would be equal.

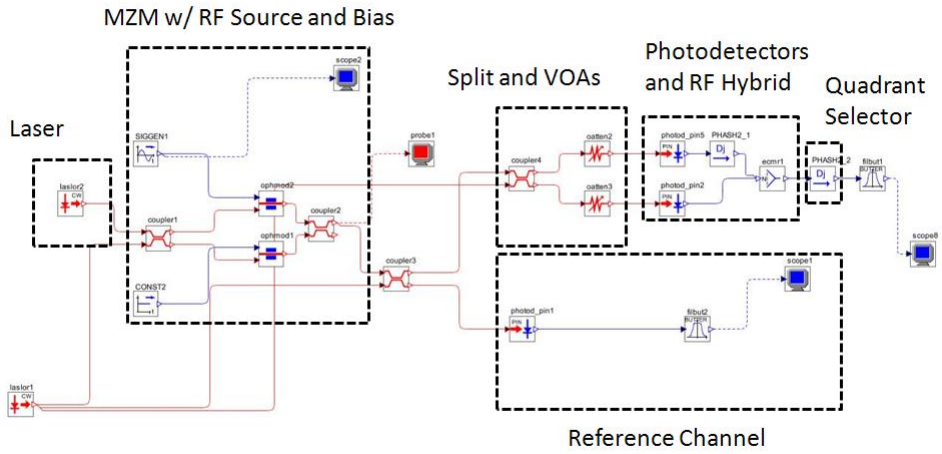

Figure 36: RSoft simulation setup for the basic two VOA design with quadrant selection.

Figure 37 shows the full 90° phase shift range in steps of about 17°. The attenuation values were chosen to maintain a constant amplitude over frequency. Because the attenuators are optical devices, the variations of amplitude and RF phase over frequency are negligible. This fact is due to the extremely small percent bandwidth of the RF to optical mapping, which has been discussed throughout this thesis. However, variations in amplitude do exist at the system level. The $3dB$ bandwidth, or roll-off, of the electro-optic modulator and photodetectors cause amplitude variation over frequency. The roll-off of MZM devices are typically smooth and the response of well designed photodetectors are usually relatively flat over the majority of the bandwidth. If amplitude variations over frequency need to be minimized, equalization of the MZM and photodetectors can be implemented. The predictable nature of the MZM and photodetector responses make equalization realizable.

While figure 37 shows the phase shifting range of 0° to 90°, figure 38 shows the quadrant selection tuning need to obtain the full 360° range. By combining the two processes and applying correct timing control, the system described can be used as a continuously tunable phase shifter. To cause vector modulation, the attenuator values can be scaled together. Figure 39 depicts multiple amplitude states while maintaining the desired phase shift.

5.1.3 Discussion

The main benefit this design offers over the optical switching network is the decrease in system complexity. The optical switching network requires control of two separate optical switches as opposed to controlling one device. For a system requiring a low number of these phase shifting architectures, controlling one device or two devices does not burden the overall system complexity significantly. However, if these architectures were used in a large phased array, doubling the amount of components to control would have a significant impact on the processing (and power) required for operation.

Another aspect of system complexity reduction lies in the amount of length matched fiber.

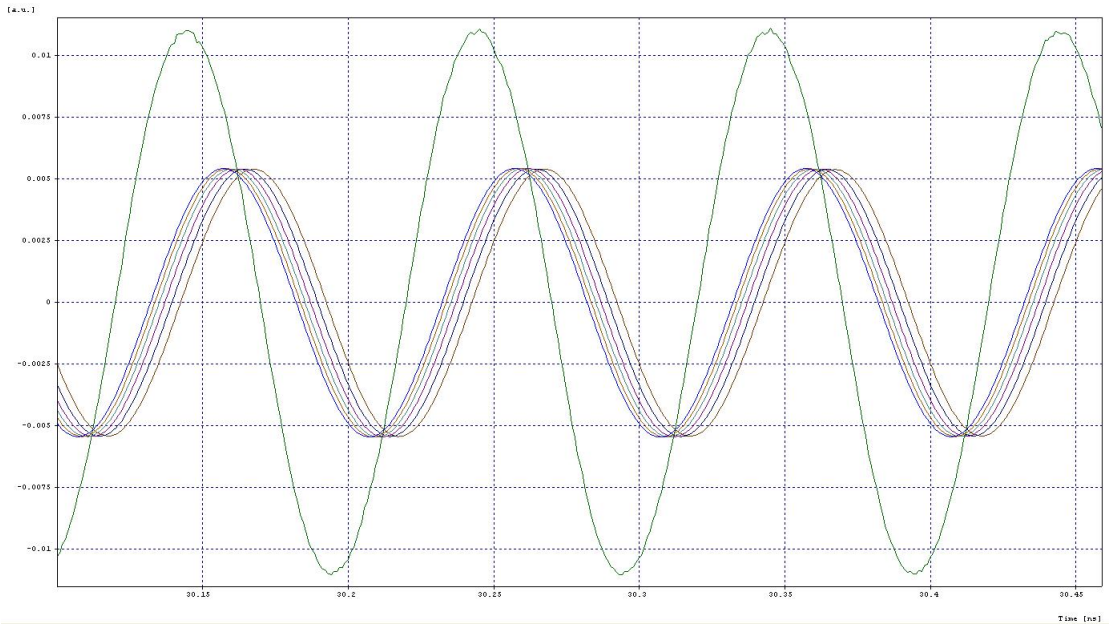

Figure 37: $10GHz$ RSoft simulation of phase shifting for the basic two VOA design with quadrant selection.

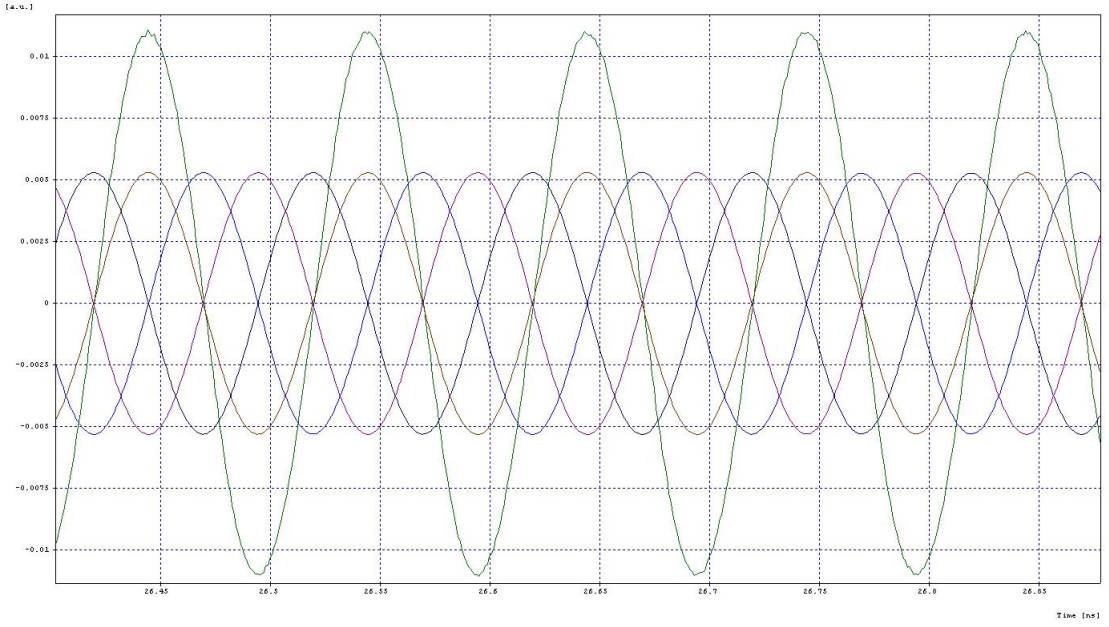

Figure 38: $10GHz$ RSoft simulation of quadrant phase shifting for the basic two VOA design with quadrant selection.

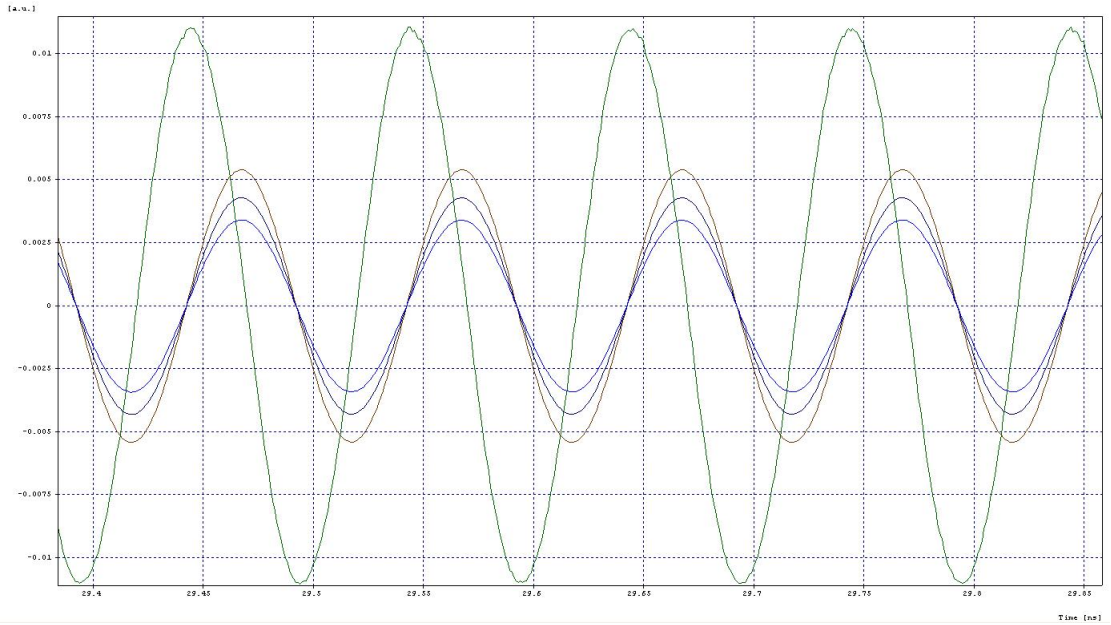

Figure 39: $10GHz$ RSoft simulation of amplitude control for the basic two VOA design with quadrant selection.

The optical switching network requires precise length matching between the MZM, $3dB$ couplers, switches, VOAs, photodetectors, and the RF hybrid input. There are six interconnecting stages of the design which require length matching. As discussed earlier, the precision of the matching is set by the upper frequency the system is design to achieve. The matching can be relaxed at lower frequencies due to the wavelength of the RF signal. However, length matching on the order of millimeters to micrometers is needed for RF signals approaching $20GHz$ and beyond.

This length matching requirement for large bandwidths causes complexity by introducing multiple calibration stages. Again, if the optical switch network was implemented with each antenna element in a large phased array, the calibration of five stages per element would become very cumbersome for manufacturing. However, as discussed earlier, optical waveguides with couplers and switches can be fabricated to make manufacturing much easier.

The proposed design cuts the number of interconnecting stages in half. This design only requires coupler-to-VOA, VOA-to-photodetector, and photodetector-to-RF hybrid interconnects to be length matched. The benefit is the decrease in system complexity which drives manufac-

turability up. Also, because there are only two complete paths that must be matched, an RF variable true time delay component can be inserted into both arms between the the photodetectors and the RF hybrid for matching the lengths even after the system has been built. Of course the lengths must be close enough for the range of the true time delays.

5.2 MZM-180°-Select, Two VOAs, and 90° Selection

5.2.1 Design

The second design utilizing variable optical attenuators and an RF hybrid is shown in the block diagram of figure 40. This design uses the 180° RF phase shifting property of the MZM to obtain the need of only a 1-bit RF phase shifter after the hybrid output. Recall from section 3 that the MZM's transfer function is a sine function, which means there is a positive sloped linear region and a negatively sloped linear region. These two regions produce an RF phase difference of 180° when the RF is electro-optically modulated onto the optical carrier. By switching between these two regions via the bias voltage and by using the same VOA-photodetector-hybrid network as in the last section, a phase coverage of 0° to 90° and 180° to 270° is obtained. Therefore, only a 1-bit selection of either 0° or 90° is required after the RF hybrid to span the full 360° needed for vector modulation.

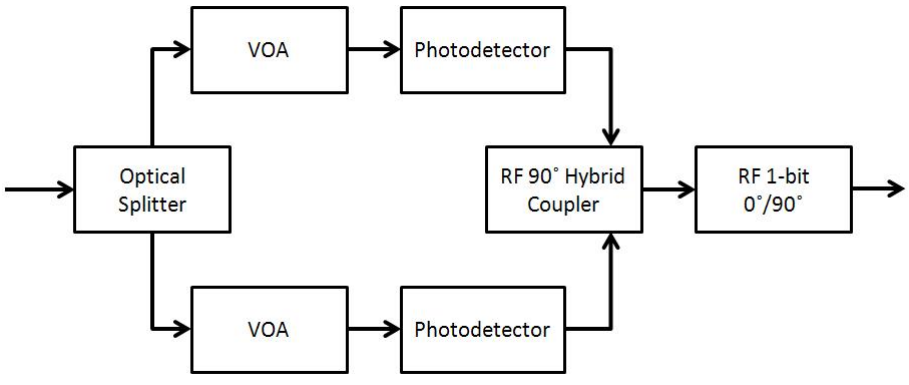

Figure 40: Block diagram of RF photonic vector modulator using modified quadrant selection.

5.2.2 Simulation

Figure 41 shows the RSoft simulation setup for the modified quadrant selection architecture using the MZM's bias voltage and a 1-bit RF phase shifter. The simulation components are the exact same as in the previous design. The difference lies with the MZM bias voltage.

Because the RF vector modulation mechanisms are the same as the previous design, only the quadrature selection was simulated. Figure 42 depicts the quadrature phase shifting capabilities. As expected, the performance is almost identical to the previous section's quadrature selection. However, these simulations assumed ideal components. The effect of real components will be addressed in the following section.

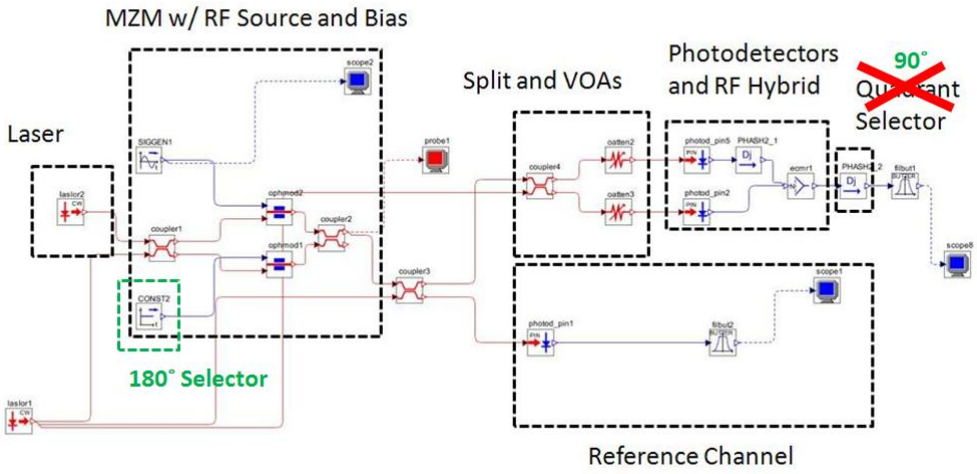

Figure 41: RSoft simulation setup of RF photonic vector modulator using modified quadrant selection.

5.2.3 Discussion

The purpose of this design is to allow more RF processing to take place in the optical domain, which is a recurring theme throughout this thesis. As was explored earlier, RF phase shifters induce unwanted amplitude and phase variations over broadband operations. This design mitigates these variations by only requiring two phase shifting states to be handled in the electrical domain. The 1-bit RF phase shifter, (or an RF 90° hybrid with a switch), needs only to select

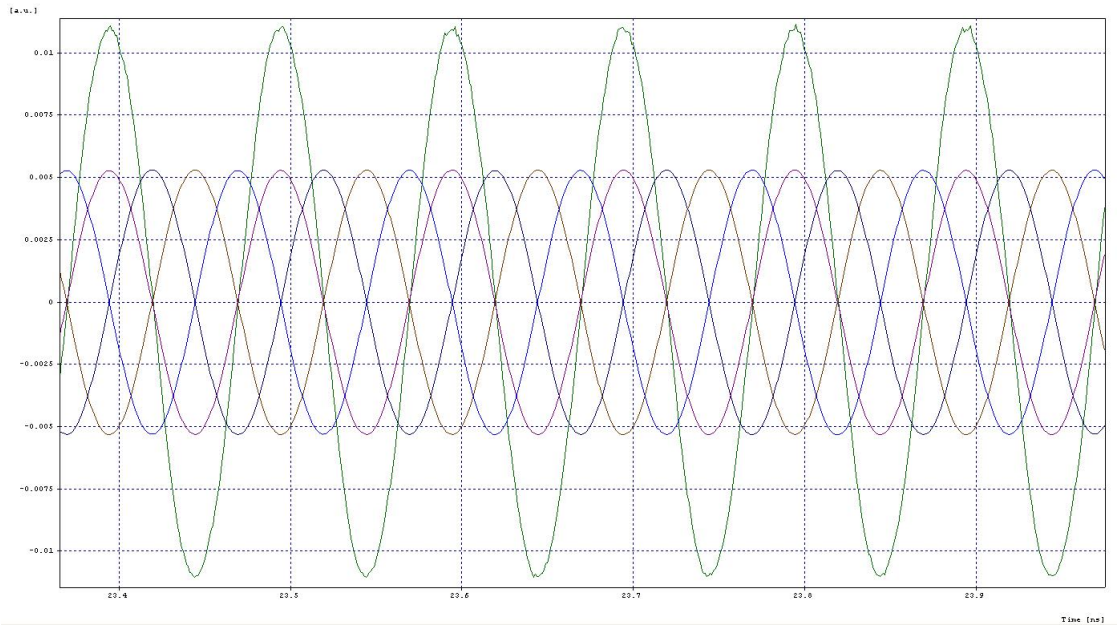

Figure 42: $10GHz$ quadrant selection RSoft simulation of RF photonic vector modulator using modified quadrant selection.

between either 0° or 90°. The reduction in the number of electrical phase states required allows more emphases to be placed on optimizing the two states needed over a large bandwidth.

Care must be taken when switching the MZM's bias voltage. Typically the voltage required will be the V_π of the modulator. The voltage applied to the MZM to cause a 180^π must be fully characterized in order to maintain amplitude and linearity. If the voltage is switched to a value with a steeper or shallower slope than the original modulation slope, then unwanted amplitude and phase changes may occur. As was discussed previously, incorrect modulator biasing will affect the spur-free dynamic range which is dependent on the linear region of the MZM's transfer function.

5.3 Two Lasers and Quadrant Selection

The next two designs make use of wavelength division multiplexing(WDM). Another huge advantage fiber optic transmission systems have over traditional electrical systems is the fact that multiple channels, or wavelengths, can be transmitted on the same fiber simultaneously with minimal channel cross talk. The following design will utilize this unique property afforded by photonics.

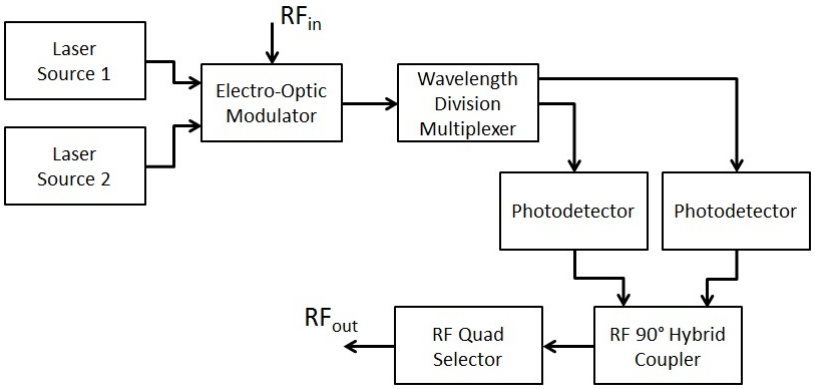

Figure 43: Block diagram of two lasers and quadrant selection RF photonic I/Q vector modulator.

5.3.1 Design

The first noticeable change in the block diagram, found in figure 43, is the absence of any VOAs. The power, or amplitude, control of the optical channels is accomplished by adjusting the lasers' powers directly. The two lasers are either coupled or wavelength multiplexed into the MZM where both optical carriers have the RF information modulated on to them. Next, the two carriers are then demultiplexed and sent to their respective photodetectors. The resulting electrical signals are then coupled through an RF hybrid and progress through an RF quadrant selector. This design can also use the 180° phase shifting capabilities of the MZM, which was used in the previous designs.

5.3.2 Simulation

In figure 44, the two lasers, at 1550nm and 1551nm, are coupled and intensity modulated by the MZM. A coupler, optical power combiner, or WDM can be used to combine the two lasers. However, the combining device typically must be polarization maintaining because of the orientation requirements for high speed MZM's. This simulation did not take polarization effects into account. The WDM after the MZM was made from a $3dB$ coupler and two optical bandpass filters centered at $1550nm$ and $1551nm$ with $3dB$ bandwidths of $50GHz$. The remainder of the system is the same configuration presented in the past sections.

The optical power in each arm entering the MZM can be controlled either by the current driving the optical sources or by an external VOA or intensity modulator. The phase shifting steps, shown in figure 45, were obtained by changing the output power of the two lasers, which simulates either changing the driving laser current or control of an internal VOA.

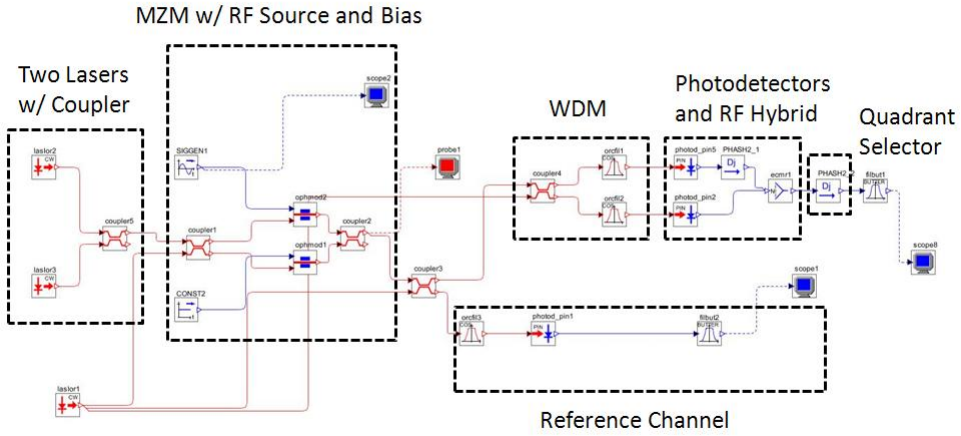

Figure 44: RSoft simulation setup of RF photonic vector modulator using two lasers and a quadrant selector.

5.3.3 Discussion

Directly controlling the laser source cuts down on the number of devices required for phase shifting in the current system architecture. However, if high speed phase shifting is required, attenuators or modulators external to the lasers may provide better system performance. One reason for this difference in performance is that internal VOAs are typically low speed compared to external VOAs and modulators. Another very important consideration is the phase noise or spectral spreading that will be added when modulating the laser's drive current. Adding external amplitude control does increase the number of components necessary for system operation; however, it can provide a "cleaner" RF phase shift and does not require length matching between the VOAs/modulators and the MZM. Recall that previous designs required length matching between all components after the MZM and up to the RF hybrid. Because the amplitude control resides outside of this length matching section in this design, the overall

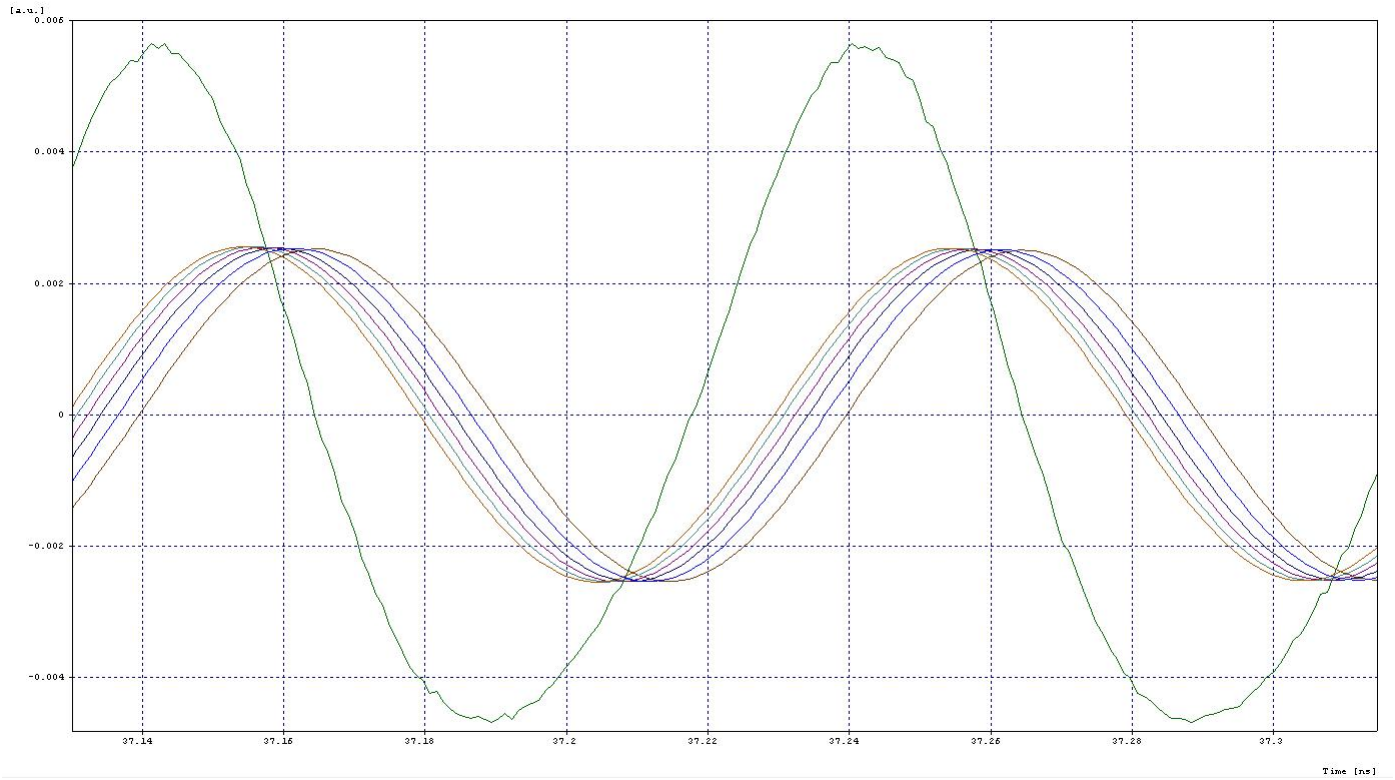

Figure 45: $10GHz$ RSoft simulation of phase shifting using two lasers and a quadrant selector.

system complexity is reduced. Again, the fiber and VOAs/modulators must be polarization maintaining if the MZM requires orientation precision and stability.

5.4 MZM Coefficient Control

The previous designs all relied on using an amplitude control device per I/Q channel. Adding components in each arm increases the complexity due to length matching requirements and can introduce error margins due to the differences in each amplitude control device. The next design uses one device to control the amplitude in both channels.

5.4.1 Design

In section 2 it was shown that a MZM has two inputs and two outputs. The transfer matrix produces two outputs with an RF phase difference of 180°. When one output is set to maximum constructive interference, meaning maximum light out, the other is set to maximum destructive interference, minimal light out. Also, when one is set to 1/2 output the other also outputs 1/2 of the input light. Therefore, by controlling only one device, amplitude in both arms can be

controlled. Figure 46 shows the block diagram of the system described.

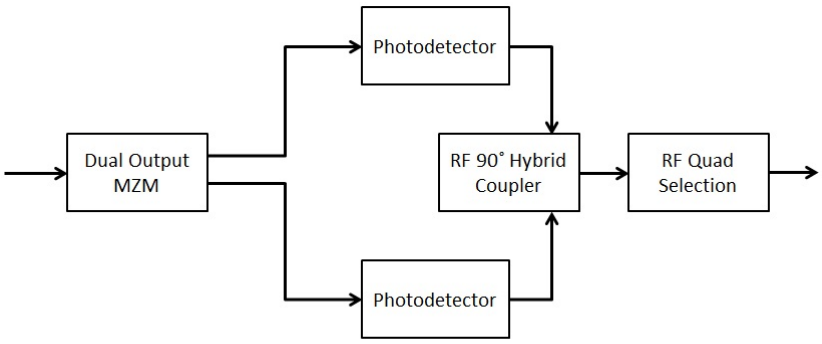

Figure 46: Block diagram of two lasers and quadrant selection RF photonic I/Q vector modulator.

5.4.2 Simulation

The simulation, found in figure 47, utilized the same setup as the two VOA system in figure **??** except that the coupler and two VOAs are replaced with one MZM device with outputs connected to the photodetectors. By changing the bias voltage to the MZM the amplitude on the I and Q channels will change resulting in a phase shift of the signal combined through the RF hybrid structure. As in previous designs, a discrete RF phase shifter alone or in conjunction with the RF modulating MZM can be used to achieve the full 360° range.

Figure 48 is the simulation result when varying the voltage of the MZM used to control the I and Q channels of the system. As shown, the amplitude variation over the phase shifting range of 90° is about 25%, which corresponds to the fact that the MZM transfer function is not equivalent to the transfer function derived in section 2 which maintains a constant amplitude over the phase shifting range.

5.4.3 Discussion

The design utilizing an MZM for amplitude control has a few advantages over the two VOA design. First, because the amplitude of the two channels are controlled by the same device, complexity is reduced. Also, mismatches between the characteristics of the two VOAs can cause undesired effects which can require calibration of operation. In the case of the MZM,

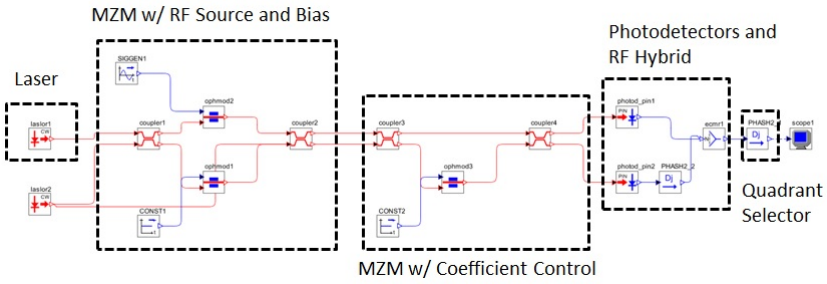

Figure 47: RSoft simulation setup of RF photonic vector modulator using MZM and a quadrant selector.

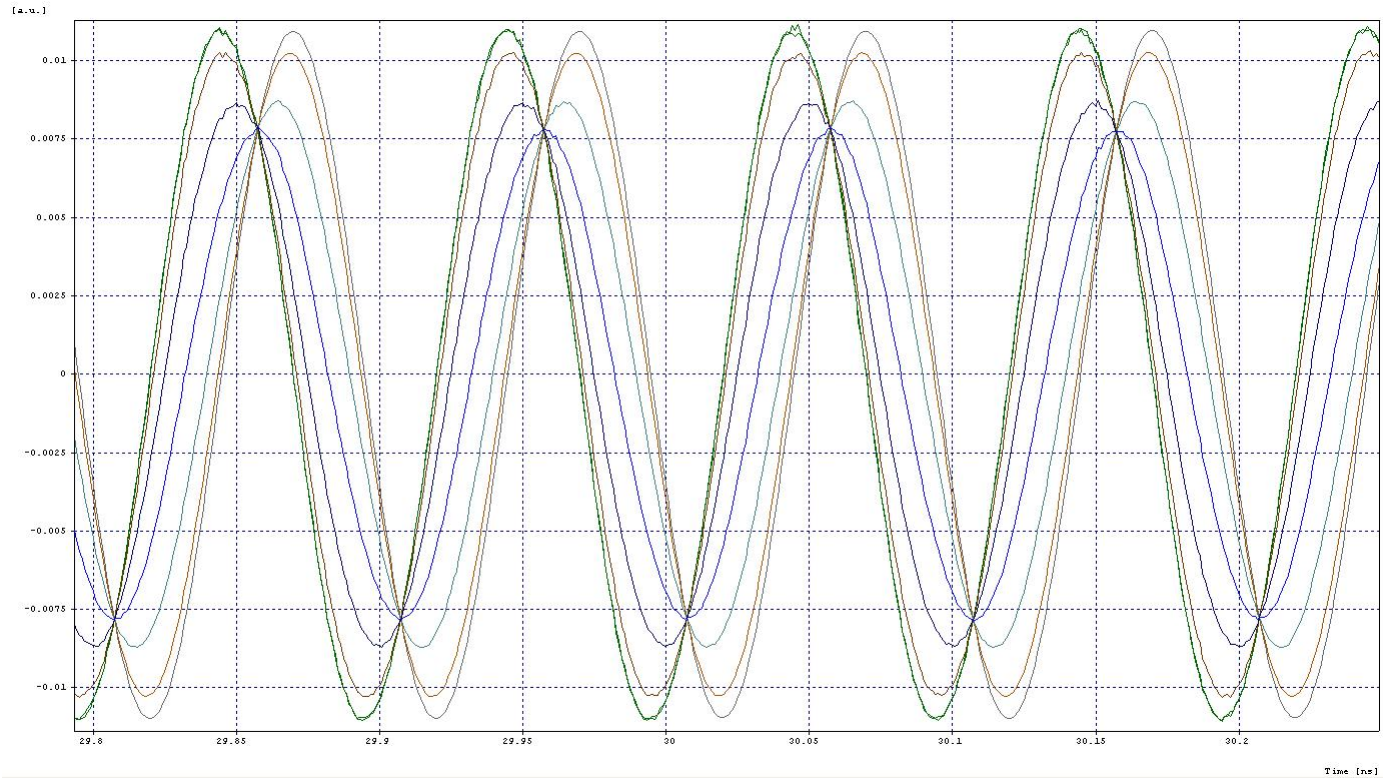

Figure 48: $10GHz$ RSoft simulation of phase shifting a MZM and a quadrant selector.

the signal response over operation remains the same if the MZM is a balanced design. Recall the 25% variation in amplitude over the phase shifting range. Using another amplitude control device will increase the device count back to two, as is the case with the two VOA design; however, because the signal passes through both the amplitude adjusting device and the MZM, the amplitude, phase, and frequency characteristics in both I and Q channels will remain nearly equal. The equivalent device operation can be expanded by using balanced photodetectors as well.

Another huge advantage is the high speed capability of MZM devices. Using a dual output MZM for I and Q means the phase can be modulated at the intensity modulation speed of the MZM, which can be greater than $40GHz$. The update rate of the MZM device exceeds state-of-the-art high speed VOAs by an order of magnitude. While this speed may be considered excessive in many applications, it has potential uses in ultra-high speed RF phase coding.

5.5 Optical Single Sideband Suppressed Carrier RF Hybrid Subset

The final potential design is actually only a subset of a full RF photonic vector modulator. This design utilizes the 90° optical phase shift of an optical $3dB$ coupler to obtain a 90° RF phase shift resulting in an optical RF 90° hybrid. The optical hybrid will be used in place of the RF hybrid to provide superior bandwidth and amplitude variation over frequency.

Optical filters have been researched extensively for their uses in the telecom industry. Many optical filters either reflect or transmit a desired range of wavelengths, which is the basis for add/drop multiplexers. Bragg gratings are used to select what wavelengths are transmitted and reflected. These filters can be used to separate the carrier wavelength from the information carrying sidebands. If the two are: separated, phase locked, have differing phases, and are then coupled back together, the overall phase shift of the combined signal will be the differing phase obtained when the two were separated. To illustrate, figure 49 shows the block diagram of an RSoft simulation. As shown, the RF information is first modulated onto the carrier. Next,

the signal is split and filtered. One arm only passes the carrier while the other only the RF information. The carrier is then phase shifted optically and coupled back together with the information carrying wave. Figure 50 shows the resulting RF phase shift due to a 90° optical phase shift. The signal displays RF amplitude noise due to the absence of optical phase locking and interference from not suppressing the carrier sufficiently. These problems can be mitigated with a phase locking system and better optical filters.

Again, by processing the RF in the optical domain the phase and amplitude variations and bandwidth are superior to the RF hybrid and RF phase shifter. However, there a few non-trivial difficulties with the optical system described. First, narrow band optical filters on the order of GHz require highly precise fabrication. Another difficulty arises from the fact that the optical filters are fixed. This means if the laser source's frequency varies near or over the cut-off of the optical filter, the information and carrier are attenuated which will greatly decrease the utility of the system. One last difficulty is maintaining a phase lock between the carrier and information. If they are not locked, increased phase and amplitude noise will be produced.

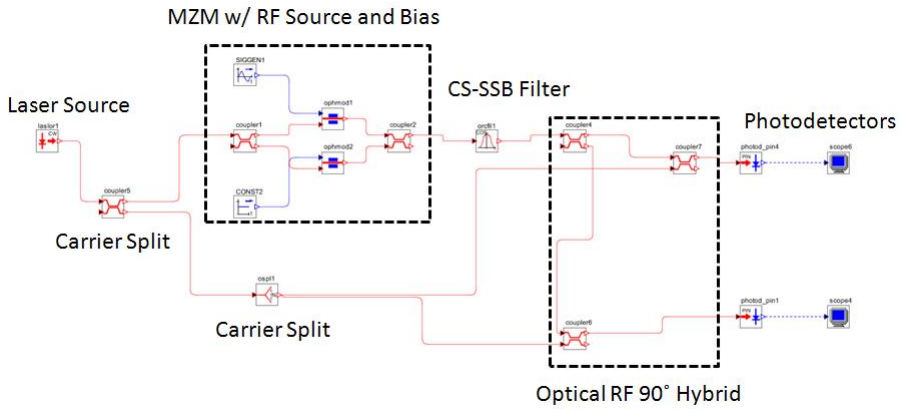

Figure 49: RSoft simulation setup for optical RF 90° hybrid

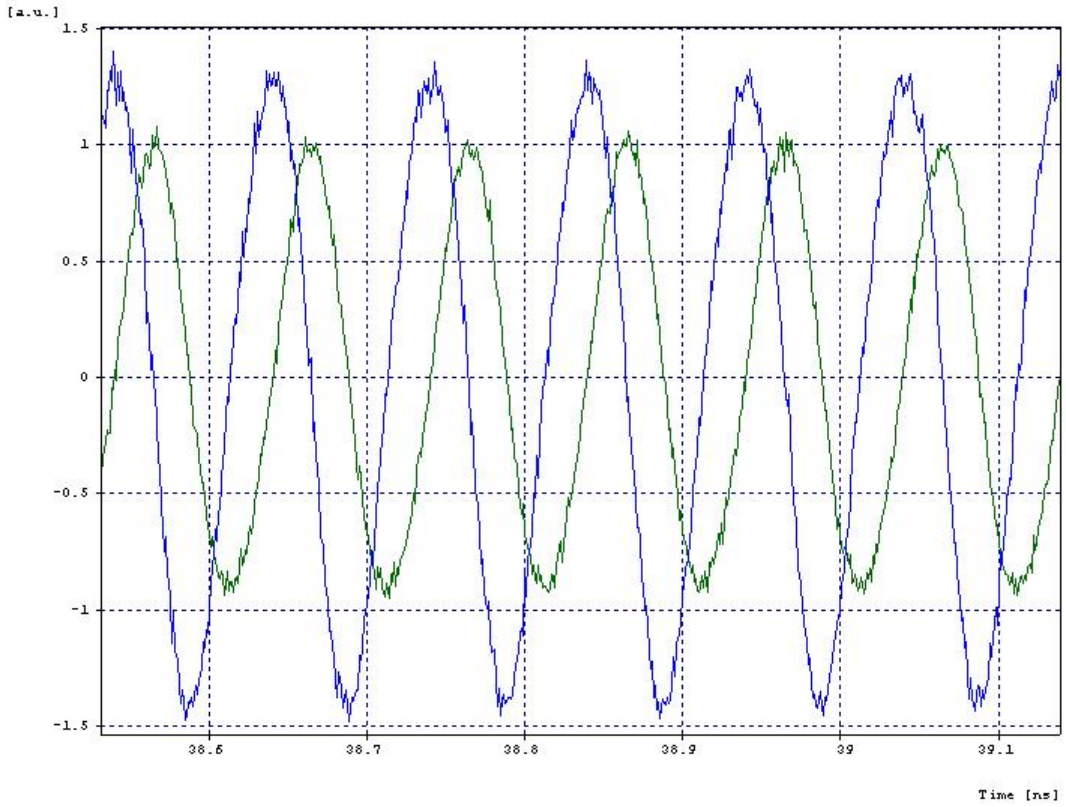

Figure 50: RSoft simulation setup for simple MZM tests.

6 NOISE FIGURE

Noise figure is a fundamental figure of merit for analog systems. In this section the noise figure will be defined and explored in a shot noise dominated photonic link and a relative intensity noise (RIN) dominated link. The derivations and definitions were referenced from [14] Chapter 5.

6.1 Noise Figure Definition

The noise figure of a device (or subsystem of devices) is a metric of how much additional noise is added to the overall system. Equation 24 gives the noise figure, NF, in dB where s_{in} is the signal power (dBm) into the system, s_{out} is the signal power out of the system, n_{in} is the noise power (dBm) into the system, and n_{out} is the noise power out of the system. This equation shows that the best noise figure possible is $0dB$, which means a system can only add noise or maintain the same amount but cannot decrease noise while maintaining the same bandwidth.

$$NF = 10log\Big[\frac{s_{in}/n_{in}}{s_{out}/n_{out}}\Big] \tag{24}$$

Equations 25 and 26 give alternate forms of s_{out} and n_{out} where g_i is the intrinsic gain of the system and n_{add} is the noise added by the system. Equation 27 is found substituting these terms into equation 24. Again, the best noise figure possible is $0dB$ which is when the noise added, n_{add}, is zero.

$$s_{out} = g_i s_{in} \tag{25}$$

$$n_{out} = g_i n_{in} + n_{add} \tag{26}$$

$$NF = 10log\Big[1 + \frac{n_{add}}{g_i n_{in}}\Big] \tag{27}$$

6.2 Shot Noise Dominated

The shot noise of a device is the random charge carrier transits over time. In the photonic systems described thus far, the source of shot noise is the photocurrent produced by the photoreceivers, making the charge carrier electrons. Equation 28 gives the current root-mean-square shot noise where $i_{rms,sn}$ is given in equation 29, q is the electron charge $-1.602 * 10^{-19}C$, τ is the time interval over which the current is measured, and I_{avg} is the average current measured.

$$i^2_{rms,sn} = \frac{|q|}{\tau} I_{avg} \tag{28}$$

$$i_{rms,sn} = \sqrt{\frac{1}{T}\int_0^T i^2_{sn} dt} \tag{29}$$

By taking the Fourier transform of the positive and negative frequencies, equation 30 is obtained showing the bandwidth dependence of the shot noise.

$$i^2_{rms,sn} = 2|q| I_{avg} \Delta f \tag{30}$$

All the systems described previously use an external MZM for RF modulation onto the optical carrier. Therefore, the noise figure will be defined for externally modulated photonic systems. Recalling equation 27, n_{add} will have two parts. The first noise source is the thermal noise of the laser, which is $g_i kT$ where k is Boltzmann's constant and T is the temperature in Kelvin. The second noise source is the shot noise of the photoreceiver given in equation 28. To obtain the noise power $i_{rms,sn}$ must be squared and multiplied by the load at the output of the photoreceiver, R_{load}. The input noise, n_{in}, is the thermal noise of the input resistance to the MZM, kT. The resulting equation using these input values is given by,

$$NF = 10log\Big[2 + \frac{i^2_{rms,sn} R_{load}}{g_i kT}\Big] \tag{31}$$

On first inspection, equation 31 shows that the noise figure can be lowered by increasing the intrinsic gain of the system or decreasing the shot noise (R_{load} is assumed to remain 50Ω and the temperature to remain near $290K$). However, the shot noise and intrinsic gain are both dependent on I_{avg}. This dependence actually results in the noise figure decreasing as the shot noise increases, which seems counter-intuitive. By working through the math found in [14], one finds that increasing the optical power increases the noise figure's numerator linearly while the denominator quadratically. The numerator of the noise figure holds the shot noise and the denominator holds the intrinsic gain resulting in the noise figure lowering as the shot noise increases.

This result seems very advantageous for photonic systems. By simply continuing to increase the amount of optical power received by the photoreceiver, lower noise figures can be obtained. There are two major problems with this path. One, photoreceivers have a limit on the amount of optical power that can be received, which also translates into the amount of photocurrent the device can handle. And two, there is a point in which the relative intensity noise of the laser will become the dominate noise source. At this point, the benefits of the shot noise case are voided.

6.3 Relative Intensity Noise Dominated

The relative intensity noise (RIN) of a photonic system is derived from the undesired power fluctuations from a laser source which translates into amplitude and instantaneous frequency noise (or phase noise). Very low RIN is highly desirable for analog photonic systems such as in long haul applications. Long haul links require high powered lasers to account for the loss over 10's of km's of fiber. Because the loss over these tremendous lengths significantly decreases the gain of the system, the laser's added noise must be low to maintain a usable signal to noise

ratio.

The RIN of a laser is due to the spontaneous emission of photons over time. Equation 32 describes the optical power noise as a function of bandwidth where the multiplication by 2 is derived from integrating the positive and negative frequencies from the Fourier transform. The rin root-mean-square of the optical power over time is given by $p_{rms,rin}(t)$ and the average optical power out of the laser is given by $P_{O,avg}$. RIN is typically used in its logarithmic form shown in equation 33.

$$rin = \frac{2p_{rms,rin}(t)^2}{(P_{O,avg})^2 \Delta f} \tag{32}$$

$$RIN = 10log\Big[\frac{2p_{rms,rin}(t)^2}{(P_{O,avg})^2 \Delta f}\Big] \tag{33}$$

To convert the RIN of the optical power to current at the output of the photoreceiver, the optical powers $p_{rms,rin}$ and $P_{O,avg}$ are both multiplied by the responsivity of the photoreceiver. Because both optical powers are multiplied by the responsivity and are squared in equation 33, the responsivity terms are cancelled and the resulting equation is given by,

$$RIN = 10log\Big[\frac{2i_{rms,rin}(t)^2}{(I_{avg})^2 \Delta f}\Big] \tag{34}$$

The noise figure for a RIN dominated externally modulated photonic system can be found by substituting $i_{rms,sn}$ for $i_{rms,rin}$ in equation 31 which gives,

$$NF = 10log\Big[2 + \frac{i^2_{rms,rin} R_{load}}{g_i kT}\Big] \tag{35}$$

The RIN of a laser source is usually given over some bandwidth. Using equation 34, $i^2_{rms,rin}$ can be found by,

$$i^2_{rms,rin} = \frac{(I_{avg})^2}{2} 10^{\frac{RIN}{10}} \Delta f \tag{36}$$

The RIN and shot noise dominated noise figures require the noise current to decrease and the gain to increase to obtain better results. It is useful to compare equations 29 and 36 due to the fact that both are dependent on I_{avg}. These equations show that the RIN is dependent on the square of I_{avg} while the shot noise dependence on I_{avg} is linear, which results in the RIN being lower than the shot noise for sufficiently low average current from the photoreceiver. However, as the laser power is increased for higher gain, the RIN will quickly over take the shot noise as the dominate noise source in the photonic link.

The trade-off analysis between gain and noise figure is very important. Some systems will sacrifice signal to noise ratio to achieve the desired signal power while other systems would rather a very high dynamic range even if the signal is very low. There are many different paths to consider such as allowing a highly sensitive RF low-noise amplifier (LNA) to apply gain after the photoreceiver. This will allow the photonic system to operate in the shot noise regime, which typically has a lower noise figure than a RIN dominate system.

All of the photonic vector modulators presented are very flexible for using different components to lower the noise figure such as LNA's, high powered lasers, high power photoreceivers, and lower V_π external modulators. The designs can also be integrated with different techniques such as low biasing and common-mode noise rejection [12, 13]. This thesis is only concerned with the fundamental mechanisms to achieve photonic vector modulation. However, noise figure considerations are vital for practical applications. Designs maximizing vector modulation control while minimizing noise figure are currently being researched but will not be included in this thesis.

7 CONCLUSION

This thesis explored the theory and design of multiple RF photonic vector modulation architectures. The benefit of applying amplitude and phase modulation in the optical domain lies in the ultra-wideband characteristics of photonic devices. Previous architectures from varying authors were presented and discussed. The physical mechanisms of these designs that resulted in RF vector modulation helped shape the new designs presented.

System complexities ranging from basic optical switched networks with variable optical attenuators to carrier suppressed single-sideband filtering with RF photonic 90 (degree) hybrid configurations were investigated. System capability versus these complexities were discussed to provide insight into tradeoffs for performance and manufacturability considerations. The main conclusion was that system complexity increases as more RF processing is pushed into the optical domain. However, much greater bandwidths are achievable with optical RF processing and RF amplitude and phase variations over frequency are less than similar all electronic ultra-wideband systems.

The final section of the thesis derived noise figure equations for basic RF photonic links. These equations are directly applicable to the RF photonic vector modulator designs because the noise figure is set by the intrinsic gain and V_π of the MZM. RF photonic systems have a lower noise figure when operating in the shot-noise limited regime. By increasing laser power into the photodetector, the noise figure is lowered. However, the is a point where the relative intensity noise will dominate over the shot-noise. Once this point is reached, the noise figure of the system is set by the phase noise characteristics of the source laser. The tradeoffs of RF photonic vector modulator designs and noise figure will be further researched but are out of the scope of this thesis.

Advanced architectures utilizing the capabilities of wave-division multiplexing, polarization

control, optical ring resonators, and specialized photodetectors are currently under investigation and offer potential alternatives to achieve enhanced performance over the architectures presented while maintaining reasonable complexity for manufacturability.

REFERENCES

References

[1] M. Richards, "Lecture 2: Radar Elements, the Range Equation, and Radar Cross Section," *ECE 6272 Fundamentals of Radar Signal Processing, Georgia Institute of Technology*, slide 22, Fall 2010.

[2] T. Sakamoto, I. Morohashi, and T. Kawanishi, "Mach-Zehnder-Modulator-Based Flat Comb Generator with Auto Bias Control," *Asia-Pacific Microwave Photonics*, pp.154-157, 2008.

[3] K. Noguchi, O. Mitomi, and H. Miyazawa, "Millimeter-wave Ti: $LiNbO_3$ optical modulators," *Journal Lightwave Tech.*, vol. 16, pp.615-617, April 1998.

[4] D. Pozar "Microwave Engineering: Third Edition," *John Wiley & Sons, Inc.*, 2005.

[5] Y. Dai, D. Fang, and Y. Guo, "A Novel Miniature 1-22 GHz 90° MMIC Phase Shifter with Microstrip Radial Stubs," *IEEE Microwave and Wireless Components Letters*, vol. 18, no. 2, February 2008.

[6] E. Chan and R. Minasian, "Photonic RF Phase Shifter and Tunable Photonic RF Notch Filter," *Journal of Lightwave Technology*, vol. 24, no. 7, July 2006.

[7] R. Nagarajan, J. Rahn, M. Kato, et al, "10 Channel, 45.6 Gb/s per Channel, Polarization-Multiplexed DQPSK, InP Receiver Photonic Integrated Circuit," *Journal of Lightwave Technology*, vol. 29, no. 4, February 15, 2011.

[8] A. Meijerink, C. Roeloffzen, L. Zhuang et al, "Phased Array Antenna Steering Using a Ring Resonator-Based Optical Beam Forming Network," *IEEE*, 2006.

[9] J. Coward, T. Yee, C. Chalfant, and P. Chang, "A Photonic Integrated-Optic RF Phase Shifter for Phased Array Antenna Beam-forming Applications," *Journal of Lightwave Technology*, vol. 11, no. 12, December 1993.

[10] S. Ristic, A. Bhardwaj, M. Rodwell, L. Coldren, and L. Johansson, "An Optical Phase-Locked Loop Photonic Integrated Circuit," *Journal of Lightwave Technology*, vol. 28, no. 4, February 15, 2010.

[11] J. Han, B. Seo, S. Kim, H. Zhang, and H. Fetterman, "Single-Chip Integrated Electro-Optic Polymer Photonic RF Phase Shifter Array," *Journal of Lightwave Technology*, vol. 21, no. 12, December 2003.

[12] E. Ackerman, G. Betts, W. Burns, C. Cox, M. Phillips, and H. Roussell, "Low-Noise-Figure Photonic Links without Pre-amplification," *Sarnoff Symposium*, pp. 1-4, 2009.

[13] J. McKinney et al., "Sub-10-dB Noise Figure in a Multiple-GHz Analog Optical Link," *IEEE Photonics Technology Letters*, vol. 19, no. 7, April 1, 2007.

[14] C. Cox, "Analog Optical Links: Theory and Practice," *Cambridge University Press*, 2004.